WINTER 2023
electronics-cooling.com

electronics COOLING

FEATURED IN THIS EDITION

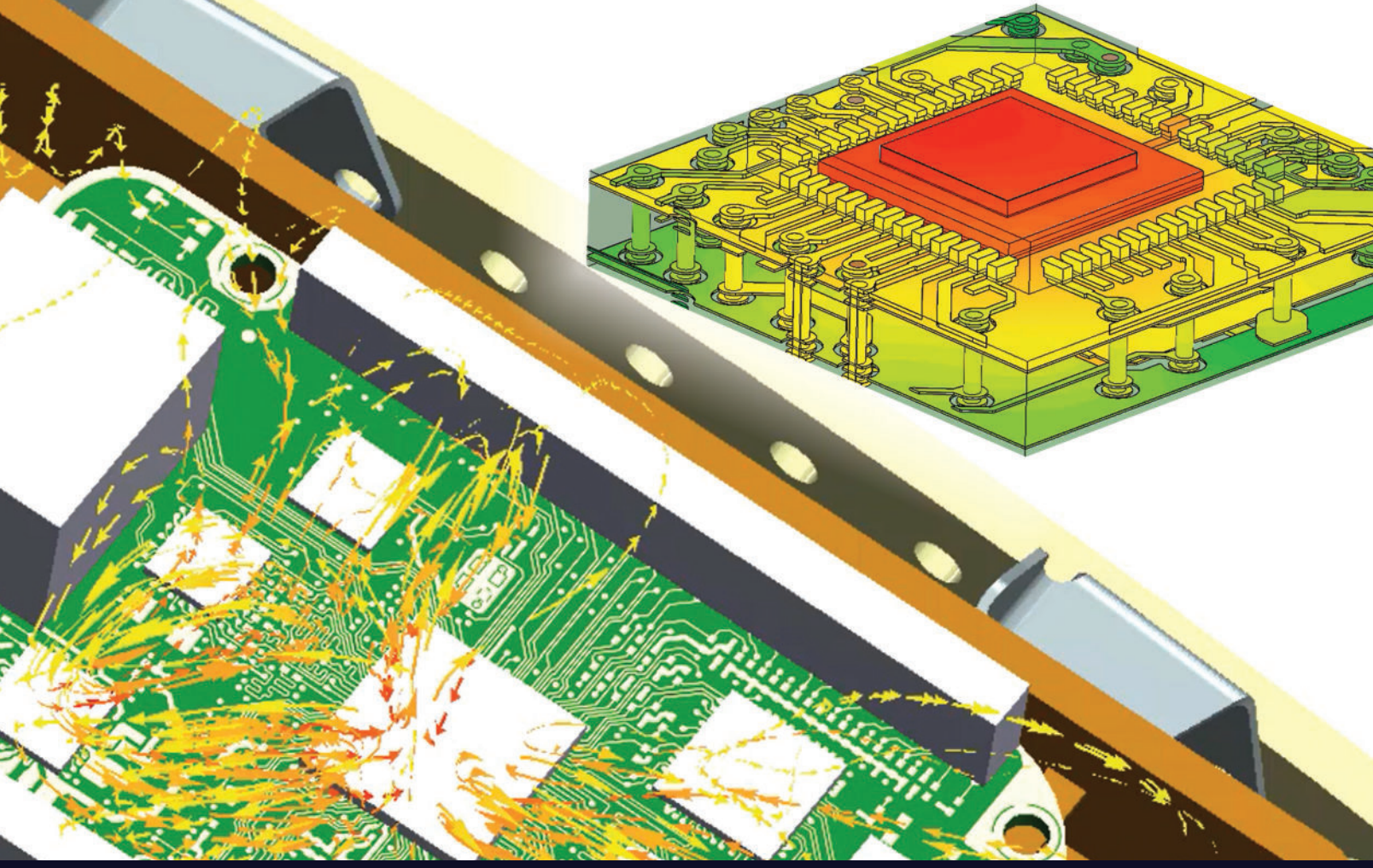

Accelerate thermal, thermo-mechanical and electro-thermal workflows

Leverage efficient CFD and FEA workflows for shorter, robust thermal and thermo-mechanical analysis. Underpin simulation accuracy with thermal measurement for characterization, calibration to reliability assessment. Incorporate EDA and MCAD data complexity efficiently into simulation. Enable PCB electro-thermal modeling using power integrity co-simulation. Realize the advantage of novel reduced order thermal model generation from full 3D analysis to improve accuracy in circuit or system modeling.

Simcenter provides simulation and test solutions to support you in developing a thermal digital twin. The portfolio includes a range of leading electronics cooling software , CAD-embedded CFD simulation options, and multi-physics analysis tools to support a wider range of user skill and experience demographic from analyst to designer. Learn how Siemens Digital Industries Software can help you achieve digital transformation goals.

www.siemens.com/simcenter

SIEMENS

CONTENTS

electronics COOLING
electronics-cooling.com

FREE SUBSCRIPTIONS

Lectrix®, Electronics Cooling®—The **2023 Winter Edition** is distributed digitally at no charge to engineers and managers engaged in the application, selection, design, test, specification or procurement of electronic components, systems, materials, equipment, facilities or related fabrication services. Subscriptions are available through electronics-cooling.com.

PUBLISHED BY
Lectrix
1000 Germantown Pike, F-2
Plymouth Meeting, PA 19462 USA
Phone: +1 484-688-0300; Fax:+1 484-688-0303
info@lectrixgroup.com
lectrixgroup.com

CHIEF EXECUTIVE OFFICER
Graham Kilshaw | graham@lectrixgroup.com

VP OF MARKETING
Geoffrey Forman | geoff@lectrixgroup.com

DIRECTOR OF MEDIA & EVENTS
Katherine Struve | katherine@lectrixgroup.com

DIRECTOR OF BUSINESS DEVELOPMENT
Ashlee Zapata-McCants | ashlee@lectrixgroup.com

CREATIVE DIRECTOR
Kate Teti | kate@lectrixgroup.com

DIRECTOR OF OPERATIONS
Stephanie Curry | stephanie@lectrixgroup.com

TRAFFIC COORDINATOR
Mackenzie Mann | mackenzie@lectrixgroup.com

CIRCULATION & ADMINISTRATION MANAGER
Eileen Ambler | eileen@lectrixgroup.com

►**SUBSCRIPTIONS ONLINE**
at electronics-cooling.com

For subscription changes email
info@electronics-cooling.com

LECTRIX

EDITORIAL

Alex Ockfen, P.E.
Associate Technical Editor of *Electronics Cooling Magazine*
Manager, Thermal & Mechanical Simulation, Meta

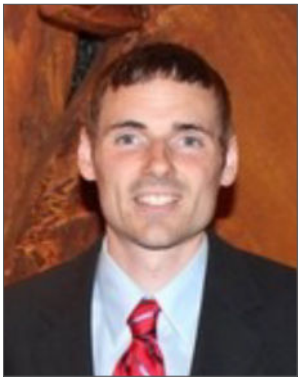

Welcome to the Winter issue of ***Electronics Cooling Magazine***.

Being a new addition to the technical editorial staff for ***Electronics Cooling Magazine***, I will start with a brief introduction. I am an engineering manager at Meta, responsible for the thermal and structural design of consumer electronics products in the augmented and virtual reality space. My current work in the consumer electronics industry followed a decade of electronics cooling in the aerospace and defense industry. Transitioning between the two industries was eye-opening, and I quickly realized that thermal challenges come in a range of shapes and sizes. The requirements for reliability, heat flux, environment, cost, etc, can vary widely. I feel lucky to have had the opportunity to contribute to a wide range of thermal designs and architectures. I look forward to continuing learning from this community, and hopefully sharing a diverse set of topics that are of interest across the electronics cooling community!

Conveniently, the exercise of writing this short introduction is an opportunity to reflect on my journey and pinpoint what led to my intersection with ***Electronics Cooling Magazine***. I quickly realized that the key to this journey has been my network. Early in my career, my network was largely limited to connections made through school or my job. This network steadily grew as I changed teams and projects, but remained limited to the aerospace and defense industry.

Once I began actively participating in conferences there was a step change in my network that started to shape and influence my career. In fact, I was first introduced to the technical editors of this magazine through the annual SEMI-THERM symposium. The friends and mentors I met at SEMI-THERM encouraged me to get involved … and I got hooked. I am honored to now be the program chair for SEMI-THERM, which is scheduled for March 2023 in San Jose. This symposium covers technical topics in areas including numerical modeling, thermal measurement methods, two-phase cooling, thermal interface materials, emerging technologies, and much more. I highly recommend attending conferences that are relevant to your work, and challenge you to find a way to participate (e.g., session chair, topic champion, reviewer). The opportunities these events have provided me, and friends made, have been immeasurable.

Okay, now back to business. First, there are a few changes to the format of ***Electronics Cooling Magazine***. The magazine is transitioning to electronic-only distribution, with no print version. This will be accompanied by an increase from three to four issues a year.

This electronic-only edition of ***Electronics Cooling Magazine*** includes a range of interesting articles that cover a diverse set of topics. We have you covered if you are interested in new thermal management applications: you will find an article on oscillating heat pipes, as well as an article on the thermal implications of LED lighting for data transfer. For those that prefer to learn something new, check out the columns on laser flash testing, the normal distribution, and thermal design power calculations for consumer electronics products.

I hope you enjoy the content in this issue. Don't hesitate to share feedback so we can continue improving. Thanks.

Alex Ockfen

KEEP IT COOL

- Thermally conductive adhesives
- Non-curing thermal compounds, greases, pastes & gels
- Dispensable thermal pads & tapes
- Liquid thermal encapsulants
- Dispensing equipment

ELLSWORTH ADHESIVES

TECHNICAL EDITORS SPOTLIGHT

Meet the 2023 Editorial Board

VICTOR CHIRIAC, PhD | GLOBAL COOLING TECHNOLOGY GROUP

Associate Technical Editor

A fellow of the American Society of Mechanical Engineers (ASME) since 2014, Dr. Victor Adrian Chiriac is a co-founder and a managing partner with the Global Cooling Technology Group since 2019. He previously held technology/engineering leadership roles with Motorola (1999-2010), Qualcomm (2010 – 2018) and Huawei R&D USA (2018 – 2019). Dr. Chiriac was elected Chair of the ASME K-16 Electronics Cooling Committee and was elected the Arizona and New Mexico IMAPS Chapter President. He is a leading member of the organizing committees of ASME/InterPack, ASME/ IMECE and IEEE/CPMT Itherm Conferences. He holds 21 U.S. issued patents, 2 US Trade Secrets and 1 Defensive Publication (with Motorola), and has published over 110 papers in scientific journals and at conferences.

► vchiriac@gctg-llc.com

GENEVIEVE MARTIN | SIGNIFY

Associate Technical Editor

Genevieve Martin (F) is the R&D manager for thermal & mechanics competence at Signify (former Philips Lighting), The Netherlands. She has worked in the field of cooling of electronics and thermal management for over twenty years in different application fields. From 2016 to 2019, she coordinated the European project Delphi4LED, which dealt with multi-domain compact modeling of LEDs and, since 2021, is coordinating the AI-TWILIGHT project. She served as general chair of the SEMI-THERM conference and is an active reviewer and technical committee member in key conferences including SEMI-THERM, Therminic, and Eurosime. She has over 20 journal and conference papers and 16 worldwide patents.

► genevieve.martin@signify.com

ALEX OCKFEN, P.E. | META

Associate Technical Editor

Alex Ockfen is a simulation engineer at Meta (formerly Facebook), providing technical leadership for thermal and structural design of consumer electronics products. He held previous positions at Raytheon where he obtained experience in thermal management and electronics cooling of a wide range of aerospace and defense applications. He has more than 10 journal and conference publications, is an inventor on multiple patents, is a professional mechanical engineer, and is currently serving as program chair of the SEMI-THERM conference.

► alex.ockfen@fb.com

ROSS WILCOXON | COLLINS AEROSPACE

Associate Technical Editor

Dr. Ross Wilcoxon is a Senior Technical Fellow in the Collins Aerospace Advanced Technology group. He conducts research and supports product development in the areas of component reliability, electronics packaging, and thermal management for communication, processing, displays, and radars. He has more than 40 journal and conference publications and is an inventor on more than 30 US Patents. Prior to joining Rockwell Collins (now Collins Aerospace) in 1998, he was an assistant professor at South Dakota State University.

► ross.wilcoxon@collins.com

COOLING EVENTS

News of Upcoming 2023 Thermal Management Events

MAR
13-17

SEMI-THERM

DoubleTree by Hilton San Jose | San Jose, CA

SEMI-THERM is an international symposium dedicated to the thermal management and characterization of electronic components and systems. SEMI-THERM provides knowledge covering all thermal scales from integrated circuits to facilities, fosters discussions between thermal engineers, professionals, and industry experts, and encourages the exchange of information on academic and industrial advances in electronics cooling.

Desc. source: electronics-cooling.com
► **semi-therm.org**

MAY
9

thermalLIVE™ SUMMIT

Online Event in EST

thermalLive Summit is a chance for thermal engineers, researchers, professionals and many more to come together to learn from industry experts on the front lines. With ongoing technology developments, this event is your chance to learn answers to questions and hear industry-leading liquid cooling technical experts' opinions and recommendations.

Desc. source: electronics-cooling.com
► **thermal.live**

JUL
3-4

ICEHTFMT 2023

Online Event in CET

International Conference on Experimental Heat Transfer, Fluid Mechanics and Thermodynamics aims to bring together leading academic scientists, researchers and research scholars to exchange and share their experiences and research results on all aspects of Experimental Heat Transfer, Fluid Mechanics and Thermodynamics. It also provides a premier interdisciplinary platform for researchers, practitioners and educators to present and discuss the most recent innovations, trends, and concerns as well as practical challenges encountered and solutions adopted in the fields of Experimental Heat Transfer, Fluid Mechanics and Thermodynamics.

Desc. source: electronics-cooling.com
► **waset.org/experimental-heat-transfer-fluid-mechanics-and-thermodynamics-conference-in-july-2023-in-prague**

Calculating Thermal Design Power for Mobile Consumer Electronics – Part 1

Alex Ockfen
Manager, Thermal & Mechanical Simulation
META

Thermal Design Power (TDP) is a term commonly used in the thermal management of consumer electronics. While the usage of this terminology may vary across the industry, it commonly refers to the amount of power that a device may dissipate indefinitely, in a given thermal environment, without exceeding the temperature limits of the device. The TDP for a consumer electronics device is of great interest because it provides physical bounds to the experience a product can deliver to the user (e.g., phone call, internet, photo capture, gaming, etc.).

Thermal design engineers often have the greatest influence on the design of a product during the development of its architecture. It is not uncommon for designs to rapidly evolve in this phase of the design cycle, with real-time changes occurring daily or even hourly. It is also not uncommon for teams to rapidly pivot between multiple concepts. Some first-order tools are essential to provide effective thermal design guidance in a fast-paced environment. Detailed finite element or computational fluid dynamics simulations are often not practical due to the timeline and lack of design maturity. TDP provides one simple and useful metric that can guide the design in the desired direction.

Calculating Thermal Design Power

Let's consider a passively cooled consumer electronics device with the common form factor of a mobile phone or tablet device. While it is possible that such a device may be limited by the junction temperature of the electronic components themselves, this is often difficult to accurately predict for an early design concept. Instead, it is common to consider that consumer electronics devices will be thermally limited at the touch surface. This is convenient because touch-temperature limits for both safety and comfort are often independent of the detailed internal design of the product and can be used for early predictions.

The most basic relationship for the thermal design power is provided in ***equation (1)***, where h is the effective heat transfer coefficient, A is the external area of the device, T_{limit} is the touch temperature limit, and $T_{ambient}$ is the ambient operating temperature. The effective heat transfer coefficient includes all relevant heat rejection modes. For consumer electronics devices, this includes contributions for convection and radiation. The reader is referred to a heat transfer text, such as reference [2], for empirical convection correlations and additional information on linearized radiation heat transfer coefficients.

$$TDP = hA(T_{limit} - T_{ambient}) \qquad (1)$$

Assuming one knows the desired operating environment, device form factor, and touch temperature limitations, the TDP is readily calculated. This equation is powerful for quick product sizing studies. The equation inherently assumes that the device is isothermal and provides an upper bound on the thermal performance of the product.

Coefficient of Thermal Spreading

Consumer electronics devices are highly constrained and must balance thermal performance against parameters such as cost, size, and wireless performance. An additional term must be added to ***equation (1)*** to account for the fact that an isothermal design is not realistic or achievable. Thus, ***equation (2)*** includes a Coefficient of Thermal Spreading (CTS) parameter.

$$TDP = hA(T_{limit} - T_{ambient})CTS \qquad (2)$$

The CTS parameter is a measure of how effectively the external surface area of a product can reject heat. The definition of CTS is provided in ***equation (3)***, where T_{avg} is the average surface temperature of the product and T_{max} is the maximum surface temperature of the product.

$$CTS = \frac{(T_{avg} - T_{ambient})}{(T_{max} - T_{ambient})} \qquad (3)$$

The value of CTS always falls between 0 and 1, with a value of 1 reverting to the ideal isothermal TDP provided in ***equation (1)***. The actual CTS achieved for any given device is dependent on design decisions including material selection, geometry, heat

source location, etc. Typical values of CTS for mobile phones fall between 0.5 and 0.8. The interested reader is referred to reference [1] for additional details on the CTS and its origins.

During the design of a new product, the CTS is often inferred based on simulations and testing of previous products. While this may be adequate when working on the next iteration of a previous product that has been thoroughly tested, it may be inappropriate for the design of a new product. Simply leveraging previous product data poses the risk of stifling new innovative solutions.

The following section provides a physics-based approach for calculating CTS during the product design cycle. Not only does this provide a means for increasing the accuracy of early TDP calculations for consumer electronics devices, but it also provides a tool for identifying design variables that can be used to achieve a desired CTS (e.g., material selection).

The following section provides an approach to calculate the CTS for products that experience in-plane thermal gradients. An approach to calculate the CTS for products with through-plane thermal gradients will be addressed in Part II of this column.

Approach for Calculating CTS with In-Plane Thermal Gradients

The notional temperature contour in ***Figure 1*** illustrates a mobile device that cannot be accurately assumed as isothermal for the purpose of TDP calculations. In-plane thermal gradients develop along the length of the device, with a hot spot visible at its center.

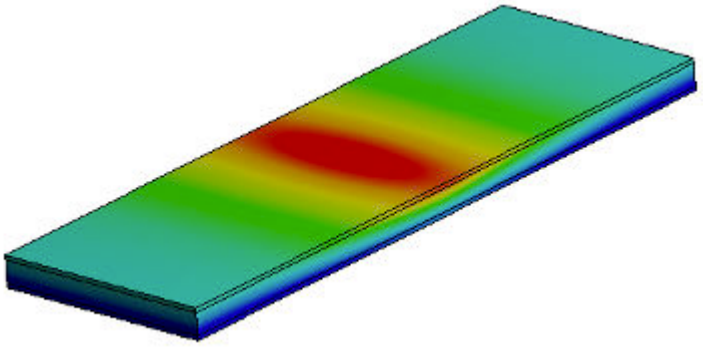

Figure 1: Isotherm on an example tablet or mobile phone product

The underlying geometry for the example device is provided in ***Figure 2*** and will be used to demonstrate the CTS and TDP calculations.

The device consists of a rectangular enclosure with a width W, a characteristic length Lc, and an enclosure thickness t. It is assumed a Printed Circuit Board (PCB) is within the enclosure, with the main heat source located at its center.

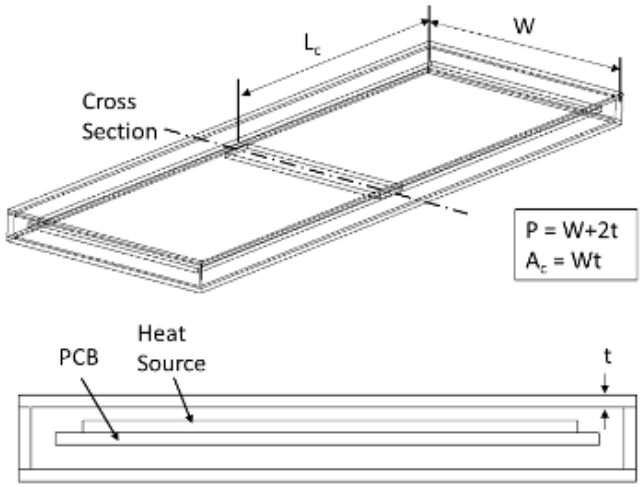

Figure 2: Example geometry of a product for demonstrating TDP calculations

Many consumer electronics devices, such as tablets and mobile phones, exhibit a form factor similar to the example geometry. The large aspect ratio of these devices is reminiscent of a fin. In ***Figure 1***, one could visualize two rectangular fins extending in opposing directions from the heat source at the center of the device. In this example, the hot spot on the enclosure corresponds to the temperature at the base of a fin, with two fins extending to either end of the product.

For large aspect ratio devices, it may also be acceptable to neglect the heat losses at the perimeter of the device because the surface area along the perimeter is often small in comparison to the surface area of the top and bottom of the device.

With these assumptions, the CTS of the device can be calculated using the fin efficiency equation for a rectangular fin with an adiabatic tip (***equation (4)***). This captures how effectively the surface area of the device can be leveraged when there are in-plane thermal gradients.

$$CTS = \eta = \frac{\tanh mL_c}{mL_c} \qquad (4)$$

Note that the characteristic length in this equation represents the distance from the heat source to the far extent of the device. In the simple example in this column, the heat source is in the center of the device and the characteristic length is half of the total length. Another possible embodiment would be to locate the heat source at the end of the device, in which the characteristic length would be the full length of the device. Thus, it is important that the characteristic length be adjusted as appropriate to the problem at hand.

The variable m in ***equation (4)*** is calculated using ***equation (5)***, where h is the combined heat transfer coefficient from the surface of the device, P is the perimeter of fin, A_c is the cross-sectional

area of the fin, and k_{eff} is the effective in-plane thermal conductivity of the device.

$$m = \sqrt{\frac{hP}{k_{eff}A_c}} \qquad (5)$$

The effective in-plane thermal conductivity may represent a single material such as a glass display or a composite stack such as a graphite layer adhered to a plastic substrate.

The perimeter in the example must be chosen to only include surfaces that reject heat to the environment. Since one surface of the fin is internal to the enclosure, it is neglected in the perimeter calculation (definition in ***Figure 2***).

The fin efficiency calculated with ***equation (4)*** quantifies how well the front and back surface areas on the device are being utilized. The fin efficiency, or in-plane CTS in this example, is plotted against the non-dimensional parameter $1/mL_c$ in ***Figure 3***. As expected, the CTS is higher when either the effective in-plane thermal conductivity increases or the size of the device decreases.

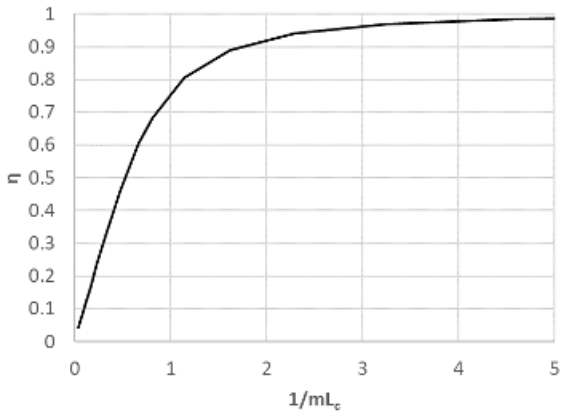

Figure 3: Fin efficiency as a function of device design parameters

Putting it into Practice

Now let's demonstrate this for the calculation of a notional device with the inputs specified in ***Table 1***. It is common for the environment, temperature limits, and desired form factor to be known.

The fin perimeter and cross-sectional areas are first calculated from the geometry definition in ***Figure 2***. For the purposes of this example, an effective heat transfer coefficient of 10 W/m^2K is assumed and accounts for both natural convection and radiation. For general situations, one can use empirical correlations [2] to refine the heat transfer coefficient for their specific circumstances. These parameters are input directly into ***equation (5)*** to calculate m, which is then input into ***equation (4)*** to calculate the CTS (or fin efficiency). Per ***Table 2***, the resulting CTS for this device is 0.55. In other words, the heat transfer from the non-isothermal surface is equal to an isothermal surface with 55% as much area.

The resulting TDP for the device, when corrected for in-plane thermal gradients, is 1.64 Watts (***Table 3***). This is lower than the ideal TDP of 3.00 Watts. If additional capability is required, the thermal designer can iterate this process to converge on a more satisfactory set of design parameters (e.g., size, material, etc.).

Table 1: Inputs for example calculation

Input	Value	Units
T_{limit}	45	°C
$T_{ambient}$	25	°C
L_c	75	mm
W	50	mm
t	1	mm
k_{eff}	20	W/mK

Table 2: In-plane CTS calculation

Parameter	Equation	Value	Unit
P	W + 2t	52	mm
A_c	Wt	50	mm^2
h	-	10	W/m^2K
m	Equation 5	22.8	1/m
$1/mL_c$	-	0.58	-
CTS	Equation 4	0.55	-

Table 3: TDP calculation

Parameter	Equation	Value	Unit
A	$4L_cW$	15000	mm^2
TDP_{ideal}	Equation 1	3.00	W
$TDP_{corrected}$	Equation 2	1.64	W

Concluding Remarks

This first-order method provides the thermal engineer with a tool to quickly estimate the thermal design power limit for devices that experience in-plane thermal gradients. This approach is well suited for architecture studies in which the design is rapidly evolving and estimates are needed to guide the design team. While this method can be very useful, it does not replace detailed design and validation. It is instead intended to refine the design concepts before transitioning to more detailed simulations and/or tests.

Since real products experience through-plane as well as in-plane thermal gradients, future work is planned to extend the approach to also account for the impact of through-plane thermal gradients.

References

[1] Victor Chiriac, "A Figure of Merit for Smart Phone Thermal Management", Electronics Cooling Magazine, April 2017
[2] Frank Incropera and David DeWitt, Fundamentals of Heat and Mass Transfer, 4th Edition, Wiley (1996)

SEMI-THERM®

39th Annual

Semiconductor Thermal Measurement, Modeling and Management Symposium and Exhibition

March 13 - 17, 2023
San Jose, CA USA

Register Now @semi-therm.org

Technical Sessions - Our Most Comprehensive Ever!

- Comfort and Compliance
- Testing & Measurement Methods (Other)
- Emerging Technology
- TIMS (Liquid Metal)
- Data Centers
- Two Phase 1
- Advanced Manufacturing & Materials
- Testing & Measurement Methods (Package)
- Immersion
- TIMS (Standard)
- Numerical Modeling Methods
- Two Phase II

Short Courses - 2 Free Courses with Full Registration

- Fundamentals of CFD for Heat Transfer Analysis: Governing Equations, Numerical Methods, and Applications
- Understanding, Applying and Estimating the Performance of Advanced Two-phase Heat Pipe Systems
- Addressing Chip Component and System Thermal and Reliability Challenges for Qualification of Automotive-Grade High-Performance Compute System
- Direct to Chip Liquid Cooling: Single Phase Water versus Pumped Two-Phase Refrigerant Cooling
- Transient Thermal Analysis Using Linear Superposition

And More

New for 2023! Facility Tour of DuPont Silicon Valley Technology Center
Monday March 13 from 6PM to 9PM

Luncheon Speakers Industry Awards Keynote Presentation Panel Discussion

Free Exhibition and Programs

New for 2023! JEDEC JC-15 Thermal Workshop
Friday March 17 from 8AM to Noon

Afternoon Exhibits Exhibitor Reception Vendor Workshops How-to Courses

View the complete program at www.semi-therm.org

Thermal Penalties of Bandwidth Enhancements for Li-Fi Communication

Anton Alexeev
EV Group

Jean-Paul Linnartz, Genevieve Martin
Signify

The rapid increase of device connectivity, coupled with constantly growing data transmission rates, increases the demand for new communication channels. Illumination systems employing Light Emitting Diodes (LEDs) have the potential to fulfill this demand. LEDs are versatile components that are used as a light source in a vast number of products: indoor and outdoor lighting, traffic signs, vehicle lights, displays, projectors, etc. At the same time, LEDs have an outstanding potential for data transmission due to their fast on- and off-switching times. Attempts to further accelerate their response is a topic of current study. This paper theoretically analyzes opportunities to increase the bandwidth to enhance data transmission rates by increasing the current density. The associated thermal penalties are estimated.

Introduction

A major trend in wireless communication is the continuously increasing carrier frequency. The increase of the carrier frequency enables the exploitation of a wider range of the spectrum and allows wider modulation bandwidths. At the same time, we see an intentional shrinking of the communication network's cell size. This enables denser reuse of the same spectrum. At low subscriber density, systems are optimized for range and coverage, which favors radio frequency (RF). With increasing user density and saturation of the spectrum, reuse and density requirements prevail. The latter favors communication by light, referred to as optical wireless communication (OWC) or LiFi [1]. The ITU g.hn g9991 standard proves to be viable in products from multiple vendors [2].

Anton Alexeev
Anton Alexeev is Business Development Manager at EV Group, where he focuses on wafer bonding technologies for a variety of applications, in particular micro-LED displays. Anton received his PhD in electrical engineering from the Eindhoven University of Technology where he also graduated a Professional Doctorate in Engineering program in physics. He has years of professional experience in the semiconductor industry. He worked on variety of technologies ranging from visible light communication via LED with Philips Lighting to optimization of the overlay performance for the leading-edge semiconductor manufacturing nodes with ASML.

Jean-Paul Linnartz
Jean-Paul Linnartz is a Research Fellow with Signify and a full professor at Eindhoven University of Technology. He and his research team work on optical wireless communication systems and on personalized human centric lighting. As a Senior Director with Philips Research, Eindhoven, he headed security, connectivity and IC design research groups. Previously, he was with the Netherlands Organization for Applied Research (TNO), TU Delft and the University of California at Berkeley. His publications are cited over 11,000 time (GS) and he has 75 granted patents. He is fellow of the IEEE for his leadership in security with noisy data, while his concept for securing IoT nodes in now used in over half a billion devices.

Genevieve Martin
Genevieve Martin (F) is the R&D manager for thermal & mechanics competence at Signify (former Philips Lighting), The Netherlands. She has worked in the field of cooling of electronics and thermal management for over twenty years in different application fields. From 2016 to 2019, she coordinated the European project Delphi4LED, which dealt with multi-domain compact modeling of LEDs and, since 2021, has coordinated the AI-TWILIGHT project. She served as general chair of the SEMI-THERM conference and is an active reviewer and technical committee member in key conferences including SEMI-THERM, Therminic, and Eurosime. She has over 20 journal and conference papers and 16 worldwide patents.

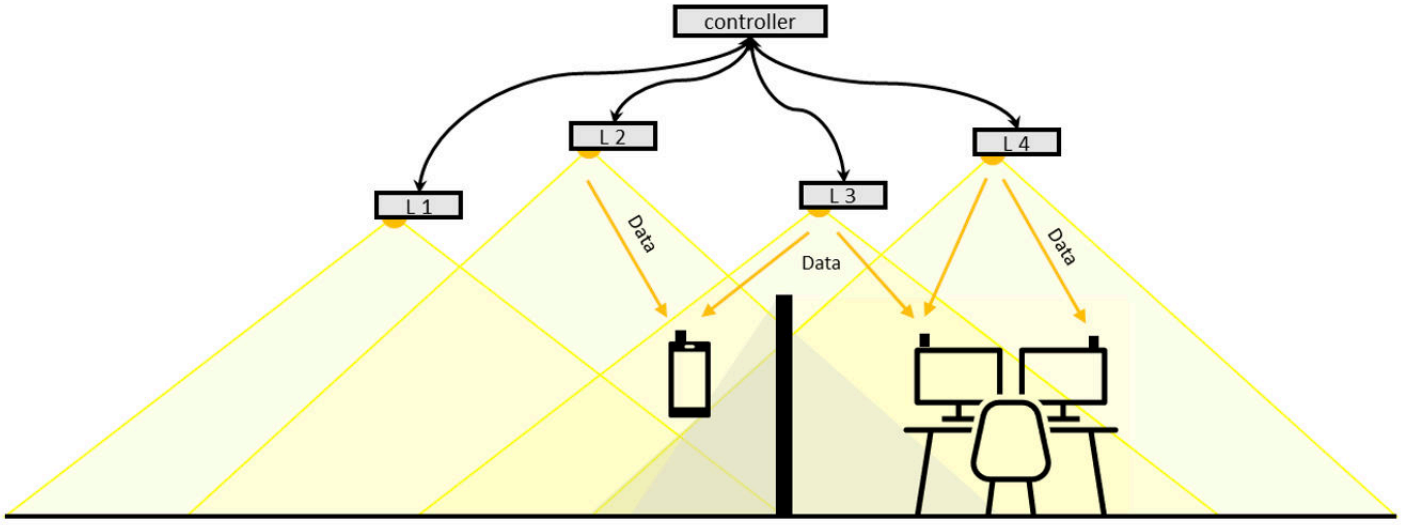

Figure 1: Illustration of a MIMO OWC system that is integrated into an SSL environment. The physical layout of the lighting system enables multiple parallel streams of data and ensures coverage.

The trend of shrinking cell sizes and the demand for low-latency communication, free of jitter from contending traffic, is well addressed by natural barriers such as walls, that allow full reuse of the light spectrum in separate rooms. The trend of moving to higher frequencies, i.e. shorter wavelengths, also makes a transition to OWC plausible.

While OWC may be vulnerable to blockage of line-of-sight propagation, distributed-multiple-input multiple-output (D-MIMO) systems with spatially separated light sources in the ceiling can provide high robustness [3]. MIMO can provide a high-bandwidth and stable connection to numerous users in crowded environments, much like the seamless shadow-free illumination that lighting systems provide.

Moreover, Li-Fi systems can reuse the light of Solid-State Lighting (SSL) LED illumination, as shown in ***Figure 1***. Indeed, the SSL infrastructure is a perfect candidate for augmentation with the OWC functionality. Lighting systems are designed to illuminate the entire environment to ensure a contiguous coverage from multiple angles. However, white illumination LEDs are optimized for (DC) illumination. Thus, they are designed for high efficiency without considering a potential need for high modulation bandwidth. Therefore, it is beneficial it turns out to be attractive to included additional light sources, in particular infra-red LEDs, to carry data [3].

The performance of the OWC channel is limited by the modulation bandwidth that is linked to the 3dB bandwidth of the LEDs [4]. By appropriately choosing LED operational parameters, the 3dB bandwidth can be enlarged. One of the possible ways to increase it is to increase the current density flowing through the pn-junction. Such an approach is common for micro-LEDs. The data transmission rates through larger LEDs can also be boosted using a similar approach. However, there is a major thermal penalty. Higher current flowing through the pn-junction affects the LED in two major ways. Firstly, it directly contributes to heat generation. Secondly, it decreases the Internal Quantum Efficiency (IQE), which leads to a higher fraction of the electrical power applied to the LED being dissipated as heat. These two reinforcing factors lead to a temperature rise of the LED package, unless they are mitigated with proper thermal management. Otherwise, the LED may not only perform less effectively but may also have a reduced lifetime or may even experience a catastrophic failure. This paper presents a theoretical analysis of this additional thermal penalty. The analysis is based on the investigation of the theoretical IQE dependence on the bias current. The IQE dependence is considered within a framework of ABC recombination model [5,6].

Dependence of the LED modulation frequency and heat dissipation on the bias current

The Multiple Quantum Well (MQW) architecture is now commonly used for highly efficient LEDs used in the illumination market. The quantum wells create narrow regions with a high concentration of holes and electrons. This facilitates the recombination processes by increasing the chance that an electron and a hole are in the same spatial region. Indeed, radiative recombination requires these two particles to be in the vicinity of each other to recombine and emit a photon. In our calculations, we model the MQW structure as a single quantum well and assume a uniform spatial density of electrons and holes inside of it. Thus, the radiative recombination rate can be modeled as a product of the second order of the MQW carrier concentration, N, and a

pn-junction design-dependent constant, i.e., $\sim BN^2$. The radiative recombination rate is proportional to the light flux. However, it is not the only recombination mechanism that takes place in the LED. It competes with the parasitic Shockley-Read-Hall and Auger recombination channels. The recombination rates of these channels are proportional to the first and the third orders of the quantum well carrier density multiplied by the corresponding material and design-dependent constants. The Shockley-Read-Hall recombination rate is proportional to $\sim AN$ and the Auger recombination rate is proportional to $\sim CN^3$. Often carrier leakage and other recombination channels are incorporated into a fourth-order term $\sim DN^4$ [7]. The fourth-order term allows better fitting of the LEDs efficiency curves at the high bias current densities.

In steady state, the total current I, flowing through an LED, can be expressed as the product of the total recombination rate and the elementary charge q:

$$I = (AN + BN^2 + CN^3 + DN^4) \cdot q$$

The Internal Quantum Efficiency IQE of an LED is defined by the ratio of the radiative recombination rate to the total recombination:

$$IQE = \frac{BN}{A + BN + CN^2 + DN^3}$$

Here, we divided out one order of N in both the enumerator and denominator. As can be seen in the previous two equations, the LED efficiency depends on the carrier concentration in the QW, which is determined by the injection current. The carrier differential lifetime τ defines the characteristic response time to a small-signal modulation. Within the ABC model framework, it is defined as [8]:

$$\tau = \frac{1}{A + 2BN + 3CN^2 + 4DN^3}$$

In the small-signal approximation, the 3dB bandwidth of the LED is proportional to the reciprocal of the differential carrier lifetime and can be expressed as:

$$f_{3dB} = \frac{A + 2BN + 3CN^2 + 4DN^3}{2\pi}$$

We see that the 3dB bandwidth depends on the carrier concentration, which in turn depends on the bias current. Therefore, the bias current directly affects the maximal modulation frequency and can be used as a knob to tweak it. Thus, the IQE, and therefore the thermal power dissipated by the LED, are also dependent on the bias current.

The thermal power dissipated by an LED can be modeled as a function of the forward voltage V, current I, IQE, and Light Extraction Efficiency LEE of the LED package:

$$P_{th} = (1 - LEE \cdot IQE) \cdot I \cdot V$$

In other words, any electrical power that is not converted into light is dissipated as heat. In our calculations, we assume a zero parasitic series resistance and a weak dependence of the forward voltage on the forward current at bias conditions above the nominal operating point, i.e., V is reasonably constant. We also assume that the LEE is constant and equal to 85%, which is a typical value for high-brightness LED packages [9].

We use the ABCD parameters of a typical commercial illumination GaN LED. The parameters were estimated and validated in [10]. We calculate the theoretical inter-dependences of P_{th}, IQE and f_{3dB}. We express the thermal power in arbitrary units for ease of interpretation.

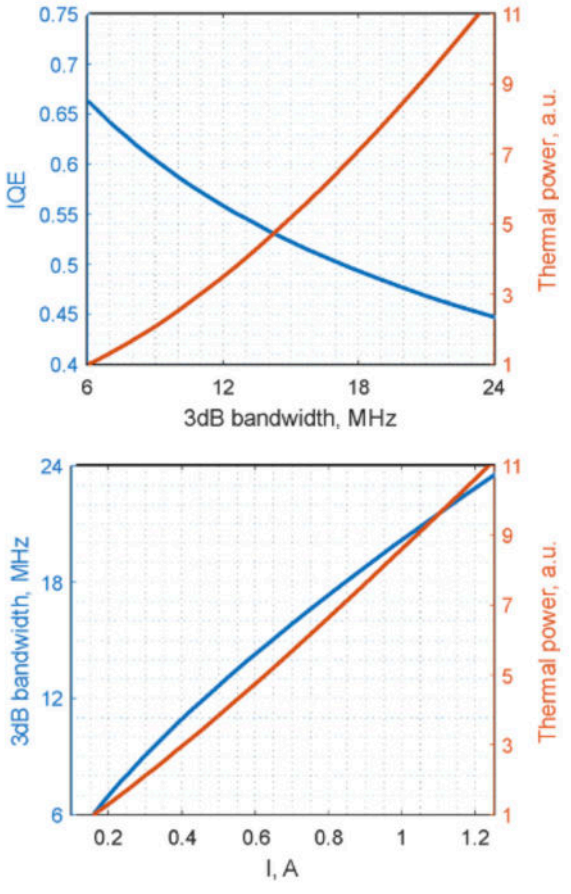

Figure 2: Interdependences of 3dB bandwidth, thermal power and forward current. The plotted minimal values of the current, thermal power and the 3dB bandwidth are correspondent to the recommended LED operation conditions.

Discussion

Data in ***Figure 2*** illustrate the characteristic dependencies of the crucial design parameters for LEDs used in SSL systems with OWC functions. We see that a bandwidth increase is possible via an increase in the bias current. Yet, this results in thermal dissipation and efficiency penalties. A twofold increase of the 3dB bandwidth from 6 MHz to 12 MHz leads to at least a threefold increase in thermal dissipation and a considerable efficiency reduction.

This demonstrates the feasibility of creating SSL luminare designs with tunable OWC properties. Such a luminare can provide both increased data rates and can retain high efficiency when it is not used for OWC. The luminaire design may incorporate multiple sets of LEDs with at least two modes of operation. In the illumination mode, the luminaire uses all the LEDs to maximize lighting efficiency. In the high-speed data transmission mode, a part of the LEDs switches off. The brightness decrease is compensated by the additional current supplied to the remaining operational LEDs. This boosts the bandwidth and therefore the data rate through these LEDs. Nevertheless, the overall efficiency of the luminare does decrease in this second mode.

Our analysis may underestimate the thermal effects and, in practice, the thermal penalty may be even higher. Specifically, our analysis assumed perfect heat sinking and ignored the fact that an increase in junction temperature causes thermal droop. One can estimate the additional drop in efficiency with observations reported in [11]. This drop is relevant to miniaturized systems with inadequate active thermal management that may not be able to cope with an increased thermal load and may not keep the LED junction temperature sufficiently low to avoid thermal droop.

Conclusions

We theoretically analyzed bandwidth tuning for accelerating data transmission in solid-state lighting systems, based on models and measurements in earlier work. The results demonstrated the feasibility of creating SSL systems with tunable efficiency and bandwidth. Nevertheless, this design may require advanced thermal management solutions to handle the additional thermal load caused by the increasing bias current at a high-speed data transmission mode. The thermal management solutions are dependent on luminaire design and may include replacing thermal plastic heat sinks with metal ones or even introducing active cooling. Finally, we have shown that the required current increase may significantly decrease the efficiency of an SSL system in this mode.

References

[1] H. Haas et al., “What Is Lifi?,” J. Lightwave Tech., vol. 34, no. 6, 2015, p. 1533–44.

[2] A.M. Khalid et al., “Productization Experiences of G.vlc (ITU) based LiFi System for High Speed Indoor Wireless Access”, Optical Wireless Communication Conference (OWCC), 2020

[3] S. M. Kouhini, S. M. Mana, R. Freund, V. Jungnickel, C. R. B. Correa, E. Tangdiongga, T. Cunha, Xiong Deng, Jean-Paul M. G. Linnartz, "Distributed MIMO Experiment Using LiFi Over Plastic Optical Fiber", IEEE Global Communications Conference (GLOBECOM), 2020

[4] J. P. M. G. Linnartz, X. Deng, A. Alexeev, and S. Mardanikorani, “Wireless communication over an led channel,” IEEE Commun. Mag., vol. 58, no. 12, 202, p. 77–82

[5] J. Cho, E. F. Schubert, and J. K. Kim, “Efficiency Droop in Light-Emitting Diodes: Challenges and Countermeasures,” Laser & Photonics Reviews, vol. 7, no. 3, 2013, p. 408–21.

[6] Q. Dai et al., “On the Symmetry of Efficiency-Versus-Carrier concentration Curves in GaInN/GAN Light-Emitting Diodes and Relation to Droop-Causing Mechanisms,” Applied Physics Letters, vol. 98, no. 3, 2011, p. 033506.

[7] M. A. Hopkins, D. W. Allsopp, M. J. Kappers, R. A. Oliver, and C. J. Humphreys, “The ABC model of recombination reinterpreted: impact on understanding carrier transport and efficiency droop in InGaN/GaN light emitting diodes,” J. Appl. Phys. 122, 2017, p. 234505

[8] A. David et al., “Carrier Dynamics and Coulomb-Enhanced Capture in III-Nitride Quantum Heterostructures,” Applied Physics Letters, vol. 109, no. 3, 2016, p. 033504.

[9] T.-p. Chen, et al., “Improvement in light extraction efficiency of high brightness InGaN-based light emitting diodes,” Proceedings of SPIE - The International Society for Optical Engineering, vol. 7216, (2009) p. 72161T

[10] A. Alexeev, et al., "Characterization of dynamic distortion in LED light output for optical wireless communications", Photon. Res., vol. 9, no. 6, 2021, p. 916

[11] I.E. Titkov et al., “Temperature-dependent internal quantum efficiency of blue high-brightness light-emitting diodes.” IEEE J. Quantum Electron 50, 2014, p. 911–920.

Utilizing Laser Flash in Combination with Finite Element Modeling to Analyze Thermal Conductivity of Interfaces and Layers within Complex Structures

Jonathan Harris
Advanced Materials Consultants AZ, LLC

Gabe Carrasco, Rutilio Olivar, Oleg Andreyko and Levi Coleman
CMC Laboratories, Inc.

Abstract

The utility of the laser flash thermal conductivity measurement can be greatly expanded to more complex structures by modeling laser flash results using Finite Element Models. This approach is illustrated using a test fixture with 4 heat sinks, where heat spreading is a significant factor. If traditional 1D thermal diffusion models for laser flash are used, thermal conductivity is significantly underestimated. By using Finite Element Models, the actual thermal conductivity can be accurately determined.

Introduction

The laser flash (LF) technique has proven to be a highly accurate method to determine the thermal conductivity of solid materials with simple geometries. The method can be applied to sheets of material as well as to layered structures and can measure thermal conductivity from 25C up to greater than 1000C.

In the laser flash technique, a pulse of laser light is used to rapidly heat the front surface of the sample of interest. As heat flows through the sample, the backside temperature rise is measured using an infrared detector. This temperature rise is fitted to a one-dimensional heat flow model that calculates the thermal diffusivity (α). The thermal conductivity (κ) is then determined by using ***Equation (1)*** below

$$\kappa = \alpha \rho C_p \quad (1)$$

where C_p is the materials heat capacity and ρ is density. If the laser pulse heating time is short compared to the backside temperature rise, and the heat flow is 1- dimensional, this model will give an accurate measurement of the material's thermal conductivity.

A schematic of the laser flash set up is shown in ***Figure 1***.

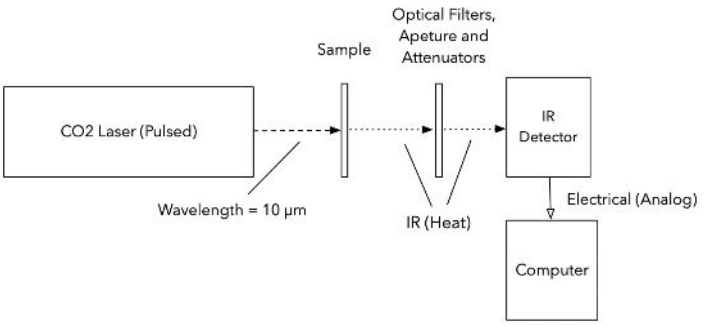

Figure 1: Laser Flash Experimental Set Up

Jonathan Harris, PhD
Dr. Harris founded CMC Laboratories, Inc., a Failure Analysis and Test Lab, in 2003. He has expertise in electronic packaging based on high thermal conductivity materials such as AlN and semiconductor assembly materials and processes. Dr. Harris sold CMC in 2022 and founded Advanced Materials Consultants, AZ, LLC. Dr. Harris has a PhD in Solid State Physics from Brown University.

Here, we utilize a CO_2 pulsed laser with a pulse length of 0.5 µsecond and a HgCdTe cooled IR detector.

As described in ASTM E1461-07[1], one of the limitations of laser flash is when heat flow through the sample is not purely one-dimensional. Even in a simple geometry, more complex heat flow can occur after laser pulse heating if heat flows laterally toward the sample edges (where convection can occur) in addition to flowing through the thickness of the sample. This is illustrated in ***Figure 2***.

If this type of non-1D heat flow occurs, the temperature rise at the backside of the sample will take longer to occur, and the fit to a 1D model will lead to a lower estimated sample thermal conductivity than the actual value.

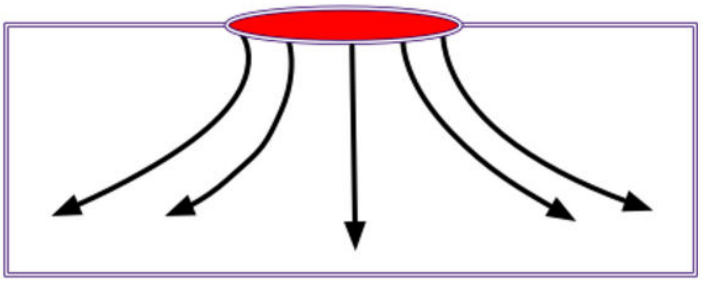

Figure 2: Non-One Dimensional Heat Flow in LF Sample

This issue is exacerbated when measuring samples with complex geometries or "real world" samples that may include heat sinks or other complicating structures.

To extend the laser flash technique to samples with more complex heat flow patterns, we have utilized Finite Element thermal simulations to model the laser flash results. As shown in this article, this approach allows us to determine the thermal conductivity of critical interfaces or material layers with unknown thermal properties within complex "real world" structures.

For simple geometries, Finite Element simulation gives the same results as a conventional 1D heat flow model. However, the Finite Element model can be extended to systems with complex heat flow induced by heat sinks and to samples with significant lateral heat flow. These are situations where the 1D model would not give accurate results.

Description of the Laser Flash Technique

As mentioned previously, the laser flash measurement uses a short laser pulse that is absorbed on the front surface of the sample. This pulse produces a very thin heated layer on the front surface that then diffuses through the sample. An IR detector focused on the backside of the sample detects the temperature rise as a function of time. This curve is the critical data output from the laser flash measurement.

In a conventional test, this temperature profile is modeled with a solution to the 1-dimension heat flow equation. This solution is shown in ***Equation (2)***, where t is the time after the laser pulse, T(t) is the time-dependent temperature of the backside of the sample, T(0) is the temperature of the sample backside at t=0, Tm is the maximum temperature of the sample backside, L is the sample thickness, and α is the thermal diffusivity[1].

$$T(t) - \frac{T(0)}{Tm} - T(0) = 1 + 2\sum_{n=1}^{\infty} -1^n \exp\left(-n^2 \pi^2 \alpha t / L^2\right),$$

Figure 2 shows an example of this backside temperature rise (red) and the fit to the 1D analytical model (white) for a graphite thermal conductivity NIST standard with thermal conductivity of 91 W/mK. An analytical solution to the 1D heat flow equation is used to fit the temperature vs. time curve to determine the thermal diffusivity, α. Thermal conductivity is then calculated using ***Equation (1)***. The material's heat capacity C_p is determined using Differential Scanning Calorimetry (DSC).

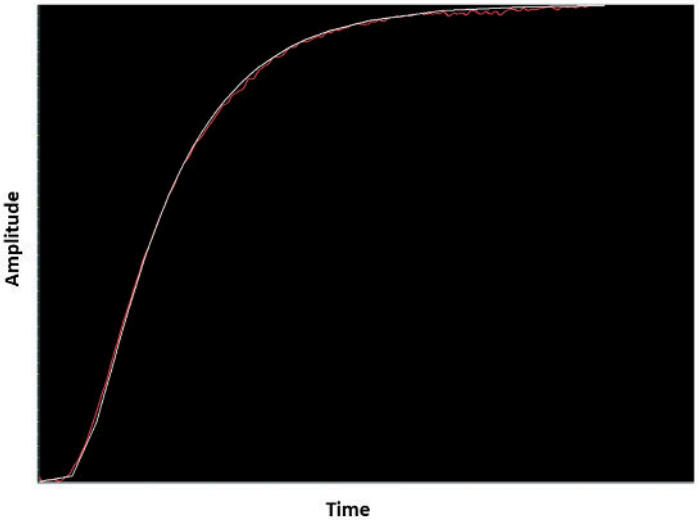

Figure 3: LF Backside Temperature vs Time and Fit to 1D Diffusion Equation

In addition to homogeneous materials, this approach can also be applied to layered structures[2]. In this case, the same type of measurement is made through the layered stack. For a three-layer structure, if the thermal diffusivities of two of the three materials are known, the diffusivity of the third material can be determined. In this case, the analytical equation for one-dimensional heat flow

[1] ASTM E1461-07, Standard Test Method for Thermal Diffusivity by the Flash Method, ASTM International, January 2008
[2] See, for example, Thermal Diffusivity of Dispersed and Layered Composites, PhD Thesis, Tsu-Yum Richard Lee, Purdue University, 1977

through a three-layer structure is used. In electronic applications, this can be very useful for determining the thermal impact of die attach or thermal interface materials (TIMs).

Finite Elements Modeling

Finite element modeling is a numerical technique that divides a body into smaller cells utilizing a mesh and then solves for properties such as mechanical stress and heat transfer at each of these finite locations. The finite element approach utilizes 3D models of the structure of interest and can thus account for complex shapes and structures that are very difficult to analyze using a single global analytical solution as is typical in conventional laser flash analysis. Commercial software programs such as SolidWorks® (utilized here) routinely perform this type of analysis.

Application to Layer Structures

In the first example, we apply both the conventional analytical 1D heat flow model and the finite element approach to laser flash measurement of an Ag epoxy die attach material sandwiched between a GaAs die and a Mo substrate. In this measurement, the thermal conductivity of the GaAs and Mo are known (measured independently), the temperature profile of the backside of the Mo is measured in the laser flash experiment, and the unknown thermal conductivity of the die attach epoxy is then determined.

In this case, heat flow through the sandwich structure is 1 dimensional, so the 1D analytical solution is a valid modeling approach. The purpose here is to show that the 1D model and the finite element model have good agreement for a situation where both are applicable.

1D Heat Flow Analytical Model Results

The results of the analytical model, as well as the material parameters input to the model, are shown below. The 1D analytical model, which analyzes 1D heat flow through a 3-layer structure, solves for the thermal diffusivity of the die attach epoxy.

Flashed Layer

Material	GaAs
Thickness	0.02314 cm
Density	5.3g/cm^3
Specific Heat (from DSC)	0.331 J/g/K
Thermal Diffusivity	0.31 cm^2/sec
Thermal Conductivity	0.5438 W/cm- K

Center Layer

Material	Ag Die Attach
Thickness	0.00309 cm
Density	3.478 g/cm^3
Specific Heat (from DSC)	0.517 J/g/K
Calculated Thermal Diffusivity	**0.0370 cm^2/sec**
Calculated Thermal Conductivity	**0.066 W/cm-K**

Rear Layer

Material	Mo
Thickness	0.01212 cm
Density	10.22 g/cm^3
Specific Heat (from DSC)	0.251 J/g/K
Thermal Diffusivity	0.241 cm^2/sec
Thermal Conductivity	0.618 W/cm-K

The 1D model calculated thermal conductivity of the Ag epoxy layer, which would include any interfacial thermal resistance, as 6.6 W/mK (calculated thermal conductivity of the Center Layer in the table).

Finite Element Model Results

A finite element model was created for the same structure. Inputs to the model included the laser pulse width of 0.5 µsec with 10 Joules of energy and the measured backside temperature vs. time after the pulse was absorbed.

The finite element model had the best fit to the measured backside temperature profile data when the thermal conductivity of the Ag epoxy layer was 6.7 W/mK. This value is very close to the 1D analytical model result of 6.6 W/mK.

An additional benefit of the finite element model is that we can also find the temperature profile for each layer as the heat diffuses, as shown in ***Figure 4***. This figure shows the initial heating of the front GaAs surface from room temperature up to about 29.85°C, transferring heat in the first 0.001 seconds to the epoxy layer with the eventual slower heating of the backside Mo layer.

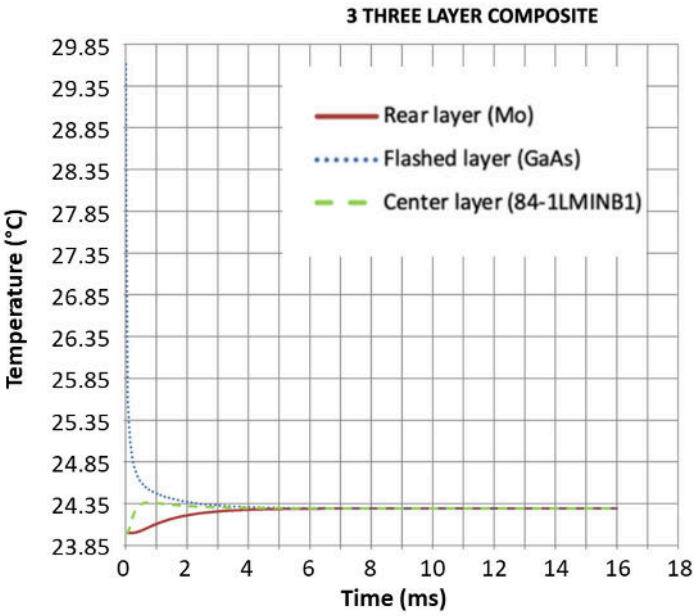

Figure 4: Temperature vs. Time for GaAs, Die Attach and Mo Layer from Finite Element Model

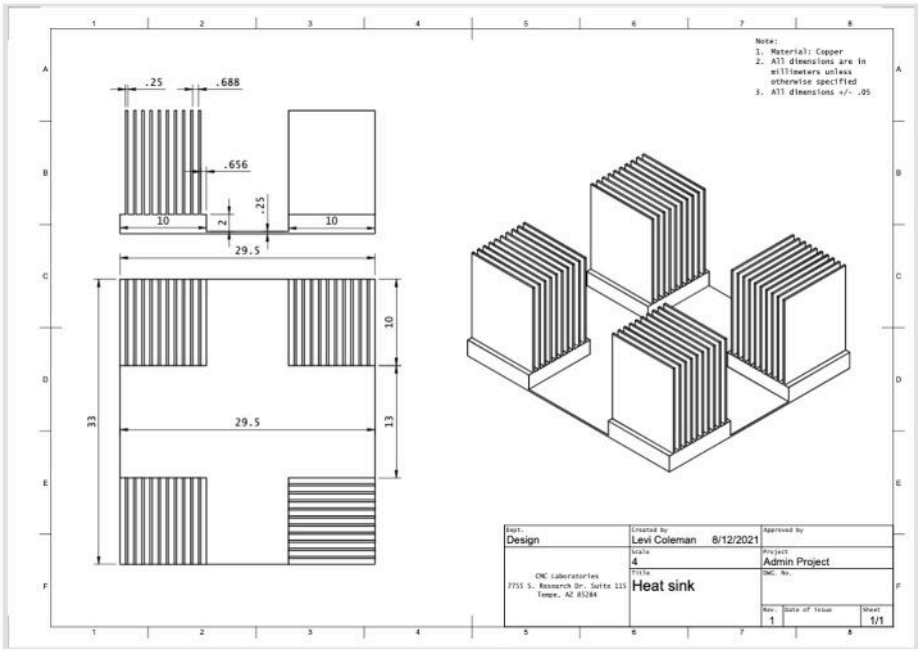

Figure 5: Test Vehicle with Lateral Heat Flow Induced by Heat Sinks

The good agreement between the analytical model for 1D heat flow and the Finite Element model in a case that is applicable to both models validates the use of the Finite Element approach to model laser flash measurements. Next, we will apply this to a more complex structure where the analytical model cannot be used.

Application to Complex Structure

Now we will apply the finite element analysis of laser flash to a complex geometry where the simple analytical model approach cannot be applied. We have constructed a test vehicle consisting of Cu substrate with 4 soldered heat sinks on each corner, as shown in the drawing above.

The laser pulse is incident on the center of the top surface and the temperature of the Cu substrate backside is measured vs. time. Before constructing this test vehicle, we measured the thermal conductivity of the bare Cu foil. The thermal conductivity of the Cu foil without a heat sink attached was 292 W/mK.

If the temperature change on the backside of the Cu foil in the heat sink structure is analyzed with the 1D heat flow model, the thermal conductivity of the Cu substrate is calculated to be 200 W/mK, which is much lower than the actual value of 292 W/mK. This drops to 160 W/mK if air is circulated over the heat sinks because of the substantial lateral heat flow toward the heat sinks. Lateral heat movement reduces the rate that the backside of the Cu heats up, which leads to a lower calculated thermal conductivity using a model that does not account for it.

With a finite element model of this more complex geometry, we can account for the lateral heat flow and convection from the heat sink surfaces. Inputs to this model are the laser power, laser pulse duration, spot size, convection coefficient from the heat sink surfaces, and the measured backside temperature rise as a function of time after the pulse is incident on the top surface of the Cu substrate.

Figure 6 shows the finite element results for the backside temperature rise, along with the measured results, for various values of the Cu substrate layer thermal conductivity. The measured data is the solid black line.

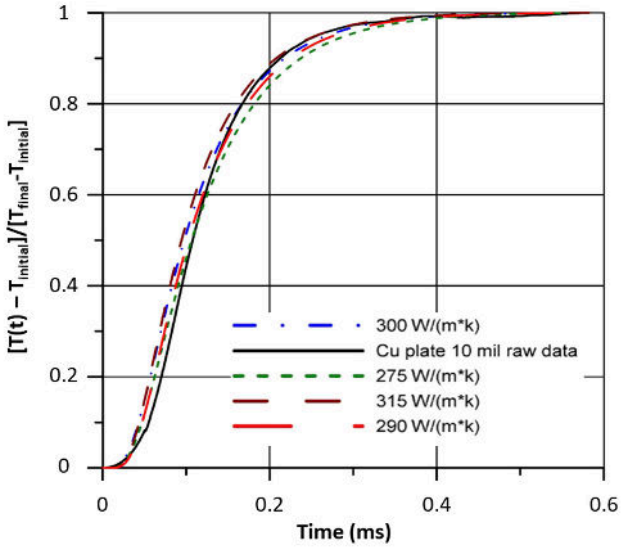

Figure 6: Finite Element Model Predictions for Backside Temperature vs Time for Different Values of the Cu Substrate Thermal Conductivity. Best Fit is for a value of 290 W/mK.

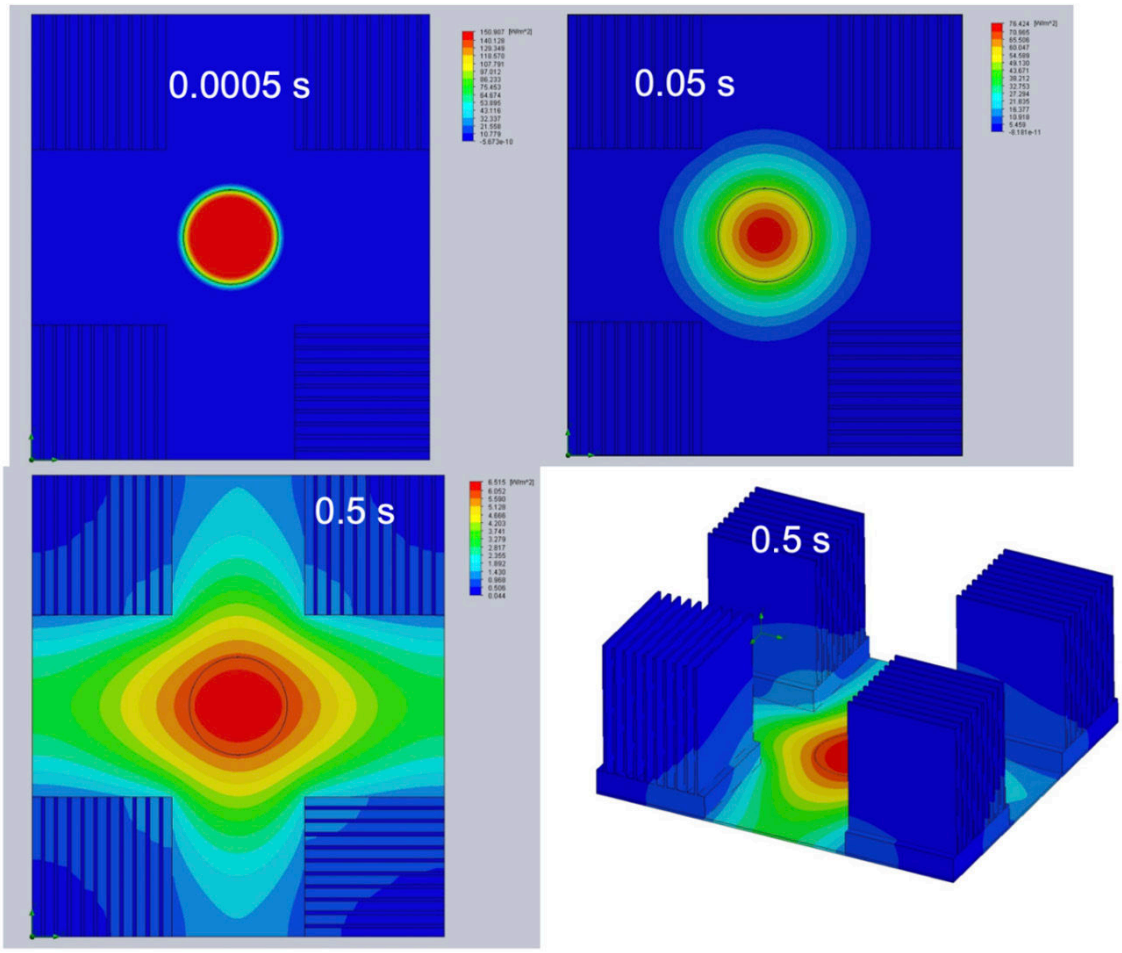

Figure 7: Temperature vs. Time for Top Surface of Cu, Cu Substrate Thermal Conductivity of 290 W/mK. From Finite Element Model.

The best fit to the actual data is a Cu thermal conductivity of 290 W/mK, which is very close to the measured value of 292 W/mK. Utilizing the finite element model with this value for the Cu thermal conductivity, we can also determine the lateral heat flow as a function of time. This is shown for the top surface in the ***Figure 7***.

This example illustrates how laser flash can be used to determine the thermal conductivity of an unknown material or interface in a complex structure where non-1D heat flow occurs. As a result, this combination of laser flash and finite element modeling greatly expands the usefulness of the laser flash measurement to "real world" geometries with complicated heat flow patterns.

Below are listed some areas of potential applications of this approach:

- Complex, irregular geometries such as geological samples
- Electronic structures with heat sinks and various heat conducting patterns as would be present in circuit board or complex packages
- Thick samples where heat flow to sample edges with subsequent convection is occurring
- Large format samples, particularly of high thermal conductivity material, where lateral heat flow is always going to be a consideration
- Complex sandwich structures with multiple layers where analytical solutions to 1D heat flow are not available

Summary

This article has shown how the combination of finite element modeling and the laser flash measurement technique can allow the thermal conductivity of materials in complex structures with non-1D heat flow patterns to be determined. This overcomes one of the major limitations of the laser flash technique.

Oscillating Heat Pipe Thermal Performance and Stability Limits

Ross Wilcoxon
Associate Technical Editor for *Electronics Cooling*
Collins Aerospace

A heat pipe is a closed system that contains a saturated fluid. When heat is dissipated in one region of the heat pipe, liquid in that area boils or evaporates, which produces vapor that moves to another area in the heat pipe where it condenses. The condensed liquid then returns to its starting point to transport energy from the heat input region(s) to the heat output region(s). The primary difference between different heat pipe technologies is the mechanism by which condensed liquid returns to the heat input regions. For example, conventional heat pipes have a wick that promotes liquid flow through surface tension. Thermal siphons rely on gravity, so their operation is greatly impacted by their orientation.

Oscillating heat pipes (OHPs), also known as Pulsating Heat Pipe (PHPs), have serpentine channels that contain the saturated fluid in discrete droplets of liquid that are randomly interspersed between pockets of vapor. ***Figure 1*** conceptually shows an OHP with a close-up view of a region of the OHP in which areas of heat input and output are indicated. Dark bubbles represent liquid droplets while white regions represent vapor pockets. Energy absorbed in the 'heat in' region, cause liquid droplets there to evaporate and become vapor. Likewise, the vapor condenses in regions where energy is removed, i.e., 'heat out' areas. These processes generate local pressure variations that cause the liquid droplets and vapor pockets to move – thereby bringing liquid into the heated regions and vapor into the cooled regions. The random distribution of liquid and vapor droplets/pockets within the serpentine path create local fluctuations in pressures, in space and time, leading to random oscillatory flow within the OHP.

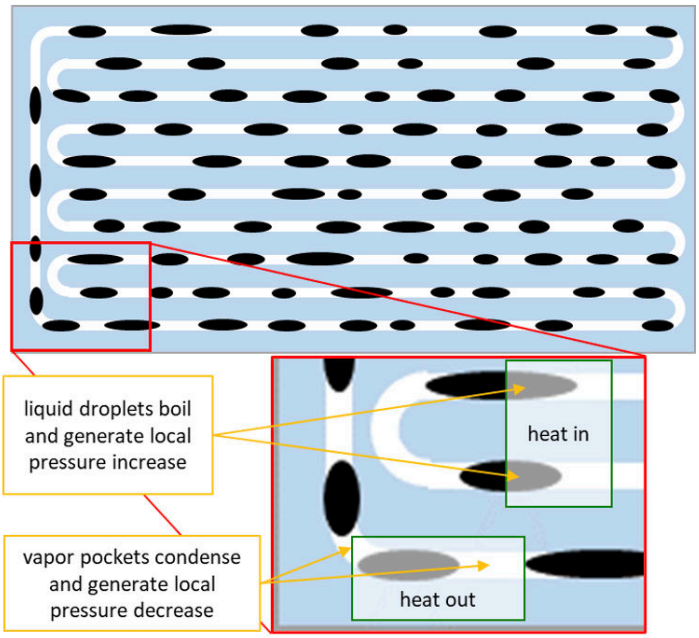

Figure 1: Oscillating heat pipe conceptual drawing

Because they rely on non-linear phenomena such as two-phase heat transfer, surface tension, etc., OHPs can exhibit non-linear behavior under different temperature and power conditions. With a proper design that accounts for the coupled effects of fluid properties and flow geometries, OHPs can stably operate over a range of conditions. Factors that influence that stable operating

Ross Wilcoxon
Dr. Ross Wilcoxon is a Senior Technical Fellow in the Collins Aerospace Advanced Technology group. He conducts research and supports product development in the areas of component reliability, electronics packaging, and thermal management for communication, processing, displays, and radars. He has more than 40 journal and conference publications and is an inventor on more than 30 US Patents. Prior to joining Rockwell Collins (now Collins Aerospace) in 1998, he was an assistant professor at South Dakota State University.

range include gravity, vapor inertia to overcome liquid surface tension, heat flux, sonic flow, fluid properties including viscosity and wetting angle, and device-specific factors such as fluid fill-fraction and evaporator/condenser lengths [1].

Many publications, including ***Electronics Cooling Magazine*** [2, 3], have discussed oscillating heat pipes. This article specifically focuses on measurements of the effective thermal conductivity of an OHP and evaluates stability conditions that define its functional operating range, as reported in Ref. [4].

This article describes testing with an OHP that was 15.24 x 2.08 x 0.40 cm (6 x 2 x 0.156 inches), made of aluminum, and filled with ammonia. Baseline testing was also done on similarly sized aluminum and copper bars, to validate the approach used to determine effective thermal conductivity.

Figure 2 shows the test configuration used for evaluating the samples. Mounting plates were attached to each end of the test bars and the OHP. These mounting plates included type T thermocouples to monitor temperatures. One end of the test sample was attached to a thermoelectric chiller that maintained the temperature of that end of the test sample. Power resistors were attached to the mounting plates fixed to the other end of the test sample to provide input power. The heaters, test sample, and thermoelectric baseplate were insulated during the tests.

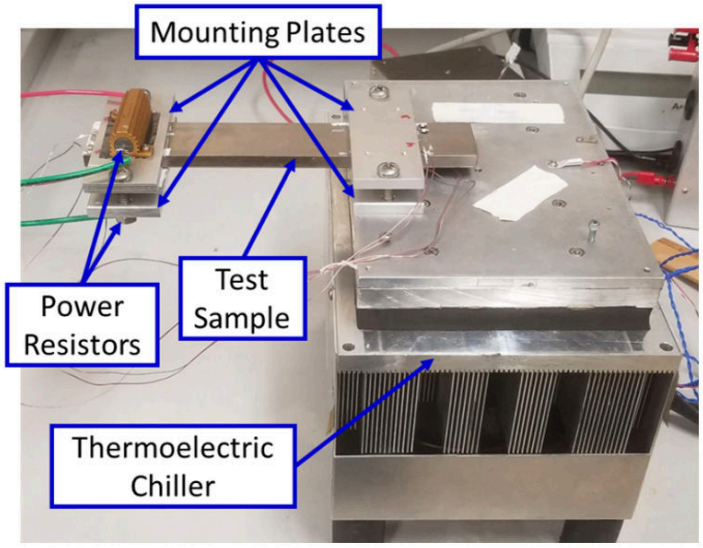

Figure 2: Thermal testing configuration

Testing was conducted by setting the thermoelectric chiller temperature to a fixed value (typically 15°C), applying a constant voltage to the heaters, and then collecting temperature data after the system had stabilized for 30-60 minutes. Data included temperatures from the thermocouples as well as the current (I) and voltage (V) from the DC power supply.

The effective thermal conductivity of a material was determined using the one-dimensional thermal conduction equation and rearranging terms to be:

$$k_{effective} = \frac{V * I * L}{t * W * \Delta T}$$

The geometric parameters t and W were fixed by the geometry of a given test sample. The length L depended on the test setup in that it was the distance between the inner edges of the two mounting plates. These plates were oriented such that the thermocouple junctions were located at these edges. Validation testing with the 7075 aluminum and copper test bars found effective thermal conductivities of ~170 and ~380 W/mK respectively. These compare well with published values for the metals, indicating that the test approach was reasonable.

Figure 3 shows plots of temperature measurements of the OHP over time for initial testing at different power dissipation values (Q) of 7.2 and 26.6W. Blue and green lines indicate temperatures of the mounting plates attached to the thermoelectric chiller while red and orange lines correspond to temperatures on the heater plates. The temperature difference (ΔT) is the average of the four heater plate temperatures minus the average temperature of the thermocouples on the mounting plate attached to the thermoelectric chiller. ***Figure 3*** shows substantially different behavior in that the OHP did not operate stably at the lower power of 7.2W, ***Figure 3a)***, but was stable when operated at the higher power of 26.6W, ***Figure 3b)***. The unstable operation at low heat input is due to non-linear relationships between boiling initiation, temperature-dependent surface tension, etc. and demonstrates that OHPs need a minimum heat input to ensure stationary, i.e., time-averaged steady state, operation.

Figure 3c) shows the effective thermal conductivities calculated from the temperature data for the power levels of 7.2 W and 26.6W. Because heat pipes have regions of nearly uniform temperature, thermal conductivity provides limited physical insight into their performance; longer heat pipes demonstrate higher effective thermal conductivity resulting from this isothermal length rather than an actual material improvement. However, effective thermal conductivity is convenient for comparing the thermal characteristics of a given heat pipe operating under different conditions. In the stable case at 26.6W, the effective thermal conductivity was relatively constant at ~2000 W/mK. The results for lower power show lower effective conductivity that oscillates between two levels of ~250 W/mK and ~1000 W/mK.

Figure 4 shows effective thermal conductivity values calculated for a range of power levels in the initial testing. In this figure, solid symbols correspond to tests in which the OHP exhibited stable operation, such as that shown in ***Figure 3b)***. Open symbols correspond to cases that exhibited unstable temperatures, similar to ***Figure 3a)***, in which the OHP thermal operation switched on and off. Two data points are plotted for each of these unstable conditions using the minimum and maximum temperature differ-

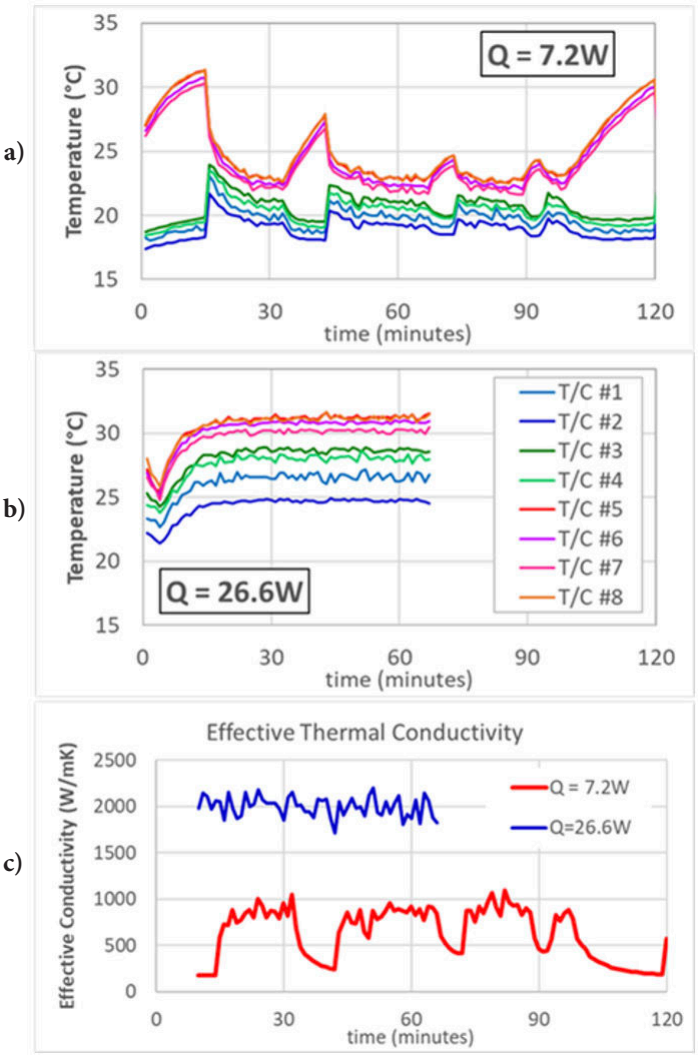

Figure 3: Examples of initial OHP testing results

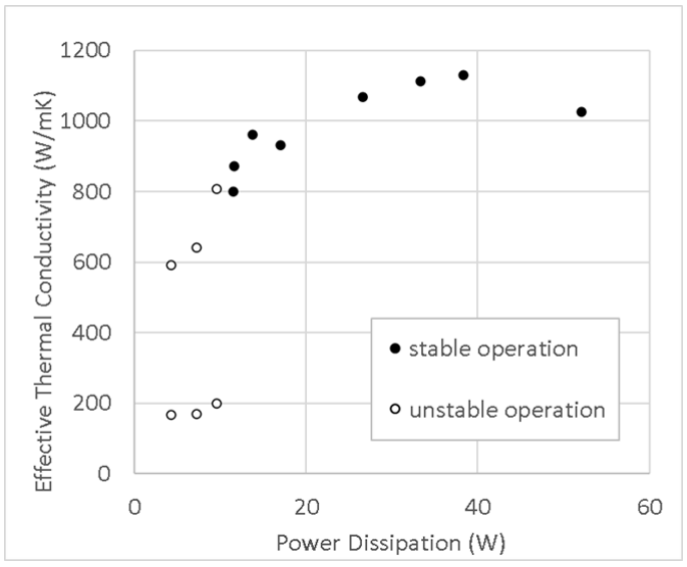

Figure 4: OHP effective thermal conductivity results: initial testing with a 15°C baseplate

ences in the unstable temperature measurements (the peaks and the valleys in the plots). In the configuration used in this testing, ~10W appears to be the power dissipation necessary for stable OHP operation.

After the initial testing, a second round of testing was conducted to push the OHP to higher power and to generate data to compare to the manufacturer's predicted maximum power and temperature limits based on approaches described in Ref. [1]. A review of the results from the initial testing revealed that they included significant effects of the temperature differences due to interfaces between the test plates and the OHP. For the second set of testing, additional thermal interface material was applied to each surface, and tests were repeated over a larger power dissipation range. Tests were conducted with the thermoelectric chiller primarily set at one of two different temperatures: 15°C and 35°C. ***Figure 5*** shows combined results for all of the test results, including the 2nd set of tests with improved thermal interfaces between the test blocks and the OHP.

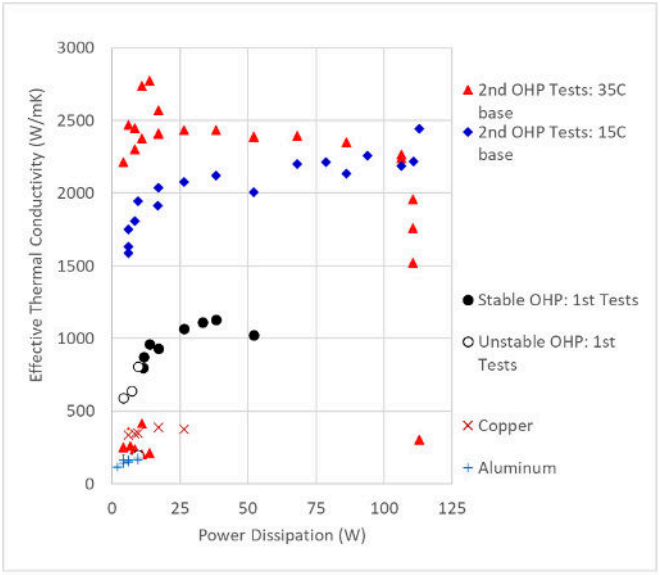

Figure 5: Combined OHP and solid materials effective thermal conductivities

Three important results are visible in this plot:

- With the improved thermal interfaces, the effective thermal conductivity of the OHP was generally 2000-2400 W/mK over the power dissipation range of 20-100 W.
- There was a substantial drop in the OHP effective thermal conductivity for lower powers, particularly with the higher baseplate temperature. This generally conforms to the ~10W threshold identified in the initial testing. However, the threshold was not as distinct as what was initially observed; instead, the unstable OHP operation occurred over a wider range of power (~5-15W).
- An additional operating limit was observed at very high powers of ~110W and with the higher temperature baseplate (35°C). This limit was not seen in the initial testing due to the maximum power dissipation of ~50W.

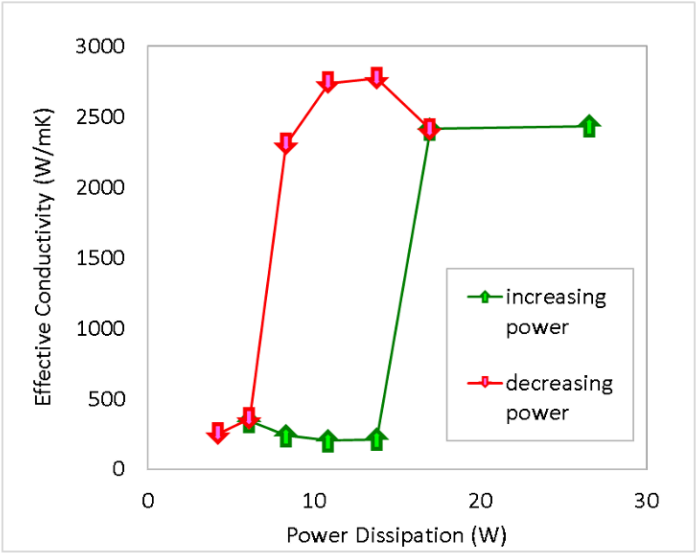

Figure 6: Hysteresis loop of the OHP operating near the startup limit (35°C baseplate temperature)

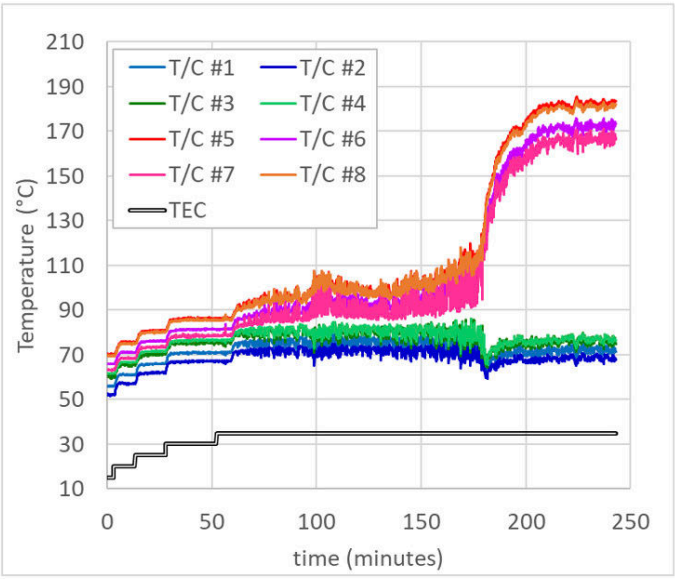

Figure 7: Results for high power and increasing cold plate temperature

As discussed in Ref. [4], the low power limit (of ~10W) is presumed to be due to the startup limit. This limit occurs when there is insufficient heat input to produce sufficient boiling to generate the pressure differential that causes fluid flow in the OHP. The startup limit primarily represents the minimum power dissipation necessary to make the OHP operate at a given temperature. The high-power limit observed in testing (~110W) is assumed to be due to the swept length limit. This limit occurs at very high heat input that causes vigorous bubble movement with insufficient amplitude of motion to maintain heat transfer. This happens when the bubbles move back and forth over a distance that is smaller than the length of the heated region – thereby not allowing the vapor bubble a chance to reach a cold spot at which it can condense.

To better understand the startup limit and particularly why it appeared to occur over a fairly wide range of powers (~5-15W), tests were conducted with the power level consistently decreased or increased after allowing the system to stabilize. In ***Figure 6***, which shows the results of this testing, the green 'up' arrows indicate the effective thermal conductivity that was determined when the power dissipation was increased after being allowed to stabilize for approximately 30 minutes. As the heat dissipation was increased from ~14 to 16W dissipation, the OHP began to operate and the effective thermal conductivity jumped from ~200W/mK to ~2400W/mK. In contrast, when power was decreased while the OHP was operating (the red 'down' arrows), the effective thermal conductivity remained high until the power was reduced from ~8 to 6W.

It is likely that the shape of the hysteresis loop shown in ***Figure 6*** would change if the stabilization time at a given power dissipation were changed from ~30 minutes. As the system approaches the start-up limit from either direction, it is likely that it would be sensitive to random fluctuations in the fluid motion that cause it to jump to the other operating condition.

To investigate the maximum power level dictated by the swept length limit, the maximum power (112.9W) of the power supply used in the investigation was applied. The temperature of the thermoelectric chiller was initially set to 15°C and the system was allowed to stabilize. The thermoelectric chiller temperature was then increased in increments of 5°C and the system was allowed to again stabilize at each temperature. This was repeated until the chiller temperature reached 35°C. Because the OHP began to then exhibit less stable operation, the thermoelectric chiller temperature was maintained to determine whether the system would stabilize. Instead, after approximately 3 hours of total test time, the OHP temperatures jumped to extremely high values as the flow channels under the heat source apparently dried out. These results are shown in ***Figure 7***.

After the end of the high-power testing that caused very high temperature for an extended period of time, the heater power supplied to the OHP was reduced to 50W. The device quickly resumed normal operation and once again demonstrated an effective thermal conductivity of ~2400 W/mK.

In conclusion, OHP testing found an effective thermal conductivity that was substantially better than aluminum or copper, as long as the OHP operated within its stable power range. Specific observations include:

- The specific OHP used in this study showed effective thermal conductivity of ~12x better than aluminum and ~5x better than copper when operating in its optimum range.

- At power levels outside the power range for stable OHP operation, the device exhbited thermal condictivity that was similar to that of the aluminum from which it was made.
- The operating range limit for the OHP depended on its operating temperature, which affects the material properties of the working fluid.
- When the power dissipation exceeded the heat input corresponding to the swept length limit, the effective thermal conductivity of the OHP substantially decreased. Once the heat input was reduced below that limit, it returned to its normal performance.

There has been substantial research activity on oscillating heat pipes in recent years. Readers whose interest has been peaked by this article are encouraged to review these developments to better understand the state of the technology to recognize whether it is appropriate for their applications.

References

[1] B. L. Drolen and C.D. Smoot, "Performance Limits of Oscillating Heat Pipes: Theory and Validation", Journal of Thermophysics and Heat Transfer, Vol. 31, No. 4, pp. 920-936, 2017, doi: 10.2514/1.T5105

[2] S. Khandekar, "An Introduction to Pulsating Heat Pipes", Electronics Cooling Magazine, May 2003, https://www.electronics-cooling.com/2003/05/an-introduction-to-pulsating-heat-pipes/

[3] J. Boswell, "Credit Card Assembly Heat Sinks with Embedded Oscillating Heat Pipes", Electronics Cooling Magazine, March 2015, https://www.electronics-cooling.com/2015/03/circuit-card-assembly-heat-sinks-embedded-with-oscillating-heat-pipes/

[4] R. Wilcoxon, J. Boswell and B. Drolen, "Oscillating Heat Pipe Thermal Performance and Stability Limits," 2022 38th Semiconductor Thermal Measurement, Modeling & Management Symposium (SEMI-THERM), San Jose, CA, USA, 2022, pp. 82-89

Summary of the IEEE ITherm 2022 Conference

John F. Maddox, Ph.D., P.E.
Associate Professor of Mechanical Engineering at the University of Kentucky, Paducah Campus

The IEEE Intersociety Conference on Thermal and Thermomechanical Phenomena in Electronic Systems (ITherm) was held at the Sheraton Hotel & Marina in San Diego, CA, May 31 – June 3, 2022. This was the 21st ITherm, which was first held in 1988. The conference was historically held every other year until 2016 when it switched to an annual schedule. ITherm 2022 was sponsored by the IEEE Electronics Packaging Society (EPS). ITherm has partnered with IEEE EPS peer conferences, including the International Workshop on Thermal Investigations of ICs and Systems (THERMINIC) in Europe, and the Electronics Packaging Technology Conference (EPTC 2022) in Asia.

The ITherm 2022 program consisted of 16 professional development workshops and three full days of technical presentations in four tracks with 48 sessions in which 173 papers were presented. Additional technical events included three keynote addresses, five panels, five technology talks, a student poster competition, and a student heat sink design competition.

Keynotes

On the first day of the conference, Dr. Vijay Narayanan, IBM Fellow and Senior Manager at IBM, gave a keynote address entitled "Accelerating Deep Learning With Analog In-Memory Compute" discussing hardware innovations to address the computational demands of the AI boom.

On the second day of the conference, Dr. Mark Jennings, Senior Technical Leader for Vehicle Energy Management & Propulsion Systems Analysis for Ford Motor Company, gave a keynote address entitled "Thermal Management Challenges for Battery Electric Vehicles" describing the challenges in thermal management system integration and vehicle connectivity.

On the final day of the conference, Dr. Tajana Šimunić Rosing, Full Professor and holder of the Fratamico Endowed Chair at the University of California–San Diego, gave a keynote address entitled "Hyperdimensional Computing System Design & Thermal Management" discussing the opportunities and challenges presented by hyperdimensional computing.

Best and Outstanding Papers

Awards given for the best and outstanding papers in each track, based on judging from reviews and inputs from session and track chairs, were unveiled to the attendees.

Professor Avram Bar-Cohen Best Papers

Component Level Thermal Management

- Amitav Tikadar, Yogendra Joshi, Satish Kumar, "Comparison between Direct Winding Heat Exchanger and Slot-liner Confined Evaporative Cooling of Electric Motor," Georgia Institute of Technology.

John F. Maddox, Ph.D., P.E.
Dr. John F. Maddox is an Associate Professor of Mechanical Engineering at the University of Kentucky, Paducah Campus. He received his Ph.D. in mechanical engineering from Auburn University in 2015. His primary research areas are thermal management of high-power electronics through jet impingement and thermal characterization of advanced materials used in aerospace and electronics cooling applications. He may be contacted at **john.maddox@uky.edu**.

System Level Thermal Management

- Quianying Wu, Todd Salamon "Two-phase thermofluidic modeling and validation of a multi-zone microchannel evaporator," Nokia Bell Laboratories and Stanford University.

Mechanics and Reliability

- Sudarshan Prasanna Prasad, Chetan Jois, Ganesh Subbarayan, "Novel Test Device for Non-destructive Experimental Characterization of Void Evolution in Microscale Solder Joints subjected to Thermal Aging," Purdue University.

Emerging Technologies & Fundamentals

- Lin Jiang, Anthony Dowling, Yu Liu, Ming-C. Cheng, "Chip-level Thermal Simulation for a Multicore Processor Using a Multi-Block Model Enabled by Proper Orthogonal Decomposition," Clarkson University.

Best Paper – Runner Up

Component Level Thermal Management

- Rahul Lall, Kamal Sikka, Isabel de Sousa, "Layered Unsupervised Learning-based Identification and Quantification of Voids in Package Thermal Interface Materials," IBM Corporation.

System Level Thermal Management

- Montse Vilarrubí, Desideri Regany, Francesc X. Majós, Manel Ibáñez, Joan I. Rosell, Josep Illa, Ferran Badia, Amrid Amnache, Éttienne Léveillé, Rajesh Pandiyan, Luc G. Fréchette, Jerome Barrau, "Numerical evaluation of bimetallic self-adaptive fins acting as flow disturbing elements inside a microchannel," University of Lleida and Universal Smart Cooling S.L.

Mechanics and Reliability

- Melina Lofrano, Bjorn Vermeersch, Herman Oprins, Seongho Park, Zsolt Tokei, "Impact of FEOL cross-heating on the thermal performance of advanced BEOL," IMEC.

Emerging Technologies & Fundamentals

- Gautier Rouaze, Jackson B. Marcinichen, John R. Thome, Kangning Xiong, L. Winston Zhang, "Pulsating Heat Pipe Fin Plates for Enhancing Natural and Forced Convection Cooling of Electronics: Experimental Campaign," JJ Cooling Innovation Sàrl.

Student Poster and Networking Session

The student poster and networking session provided an opportunity for students to interact with industry and academic leaders in their fields. This venue enabled students to connect with possible future employers and to receive feedback on their work. The student posters were subjected to two rounds of judging based on technical merit, clarity, self-sufficiency of the content, originality of the work, visual presentation, and oral presentation with best and outstanding posters selected for each technical track, and one poster was selected as the best overall.

Best Overall Poster

- Chetan Jois, Purdue University "Phase Field Simulations of Solder Void Evolution under Thermal Aging"

Best Posters

Component Level Thermal Management

- Amitav Tikadar, Georgia Institute of Technology "Comparison between Direct Winding Heat Exchanger and Slot-liner Confined Evaporative Cooling of Electric Motor"

System Level Thermal Management

- Tayler Shelly, Purdue University "A Dynamic Co-Simulation Framework for the Analysis of Battery Electric Vehicle Thermal Management Systems"

Mechanics and Reliability

- Chetan Jois, Purdue University "Phase Field Simulations of Solder Void Evolution under Thermal Aging"

Emerging Technologies & Fundamentals

- David Coenen, KU Leuven "Circuit-level thermal modelling of Silicon Photonic Transceiver Array using Machine Learning"

Outstanding Posters

Component Level Thermal Management

- Aaron Smith, Auburn University "Flow Visualization of Turbulent Jet Impingement with Engineered Surface Modifications through Particle Image Velocimetry"

System Level Thermal Management

- Veeresh Ayyagari, University of Maryland College Park "Performance Characterization of a Novel Low-Cost Additively Manufactured PCM-to-Air Polymer Composite Thermal Energy Storage for Cooling Equipment Peak Load Shifting"

Mechanics and Reliability

- Jinesh Narangaparambil, Auburn University "Influence of Component Interconnect with Printed Copper Circuits on Realized Mechanical and Electrical Characteristics in FHE Applications"

Emerging Technologies & Fundamentals

- Maureen Winter, Purdue University " The Effect of Fin Array Height and Spacing on Heat Transfer Performance during Pool Boiling from Extended Surfaces"

Student Heat Sink Design Challenge

The ASME K-16/IEEE EPS Student Design Challenge is a team competition in which students design, analyze, and optimize an additively manufactured, aluminum heat sink to cool a constant heat flux power electronics module subject to natural convection. Designs were submitted by teams from around the world and evaluated by a team of experts based on a series of design and manufacturing criteria. For the 2022 competition, the top 7 most effective and creative designs were printed using additive manufacturing facilities at GE and tested using state-of-the-art test equipment at the University of Utah. The 7 finalist heat sinks are shown in ***Figure 1***.

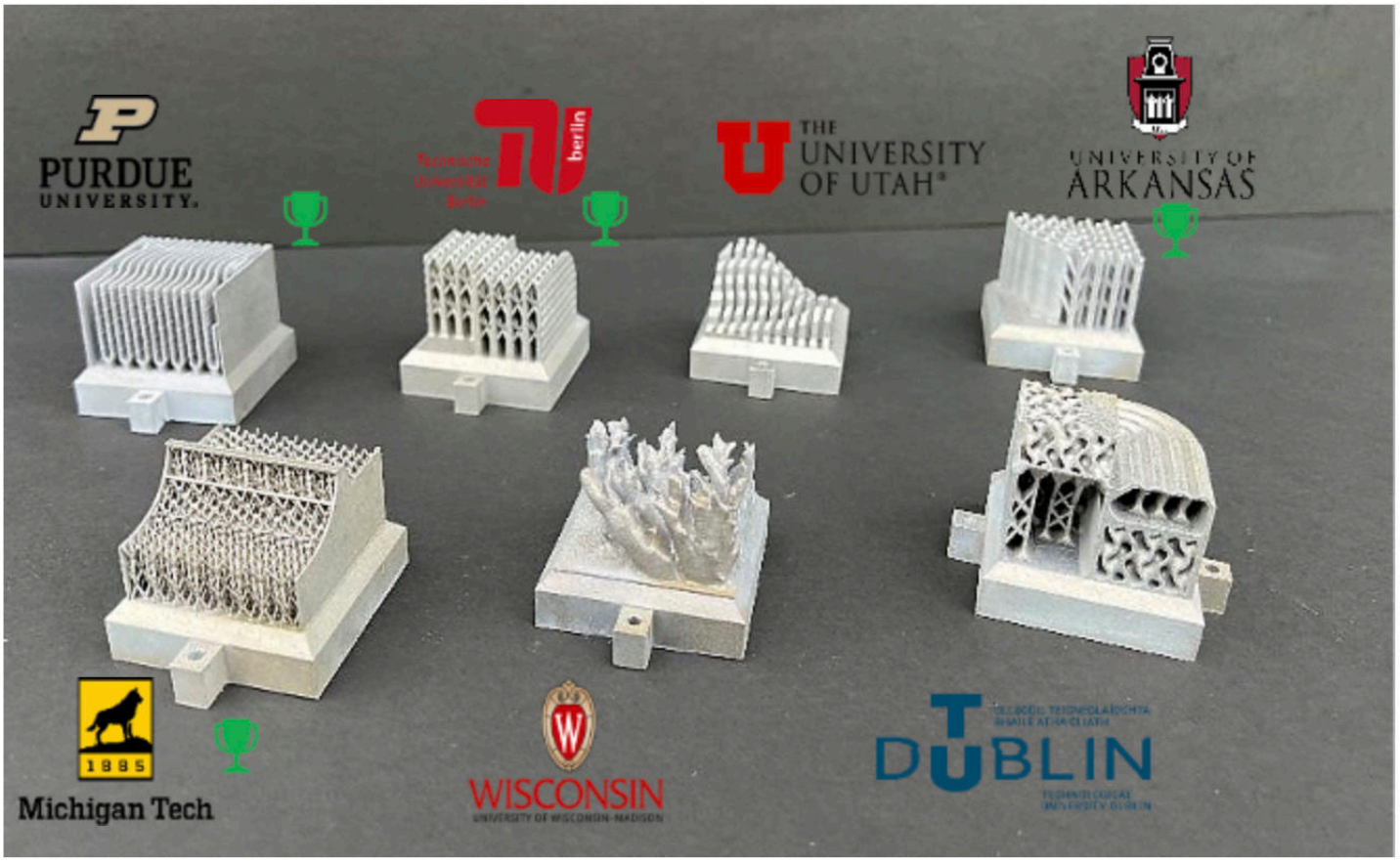

Figure 1: Heat sink design challenge finalists. [Top row left to right: Purdue University, Technische Universität Berlin, University of Utah, University of Arkansas; Bottom row left to right: Michigan Technical University, University of Wisconsin, Technological University Dublin]

Winner

- Alexander Nicolai, Lisa Stencel, Diego Montalvo, Eike van Dieken, Technische Universität Berlin (***Figure 2***)

Runner-up

- Behzad Ahmadi, Kelsey Brinks, Masoud Ahmadi, Gracie Brownlow, Behnam Ahmadi, Michigan Technical University (***Figure 3***)

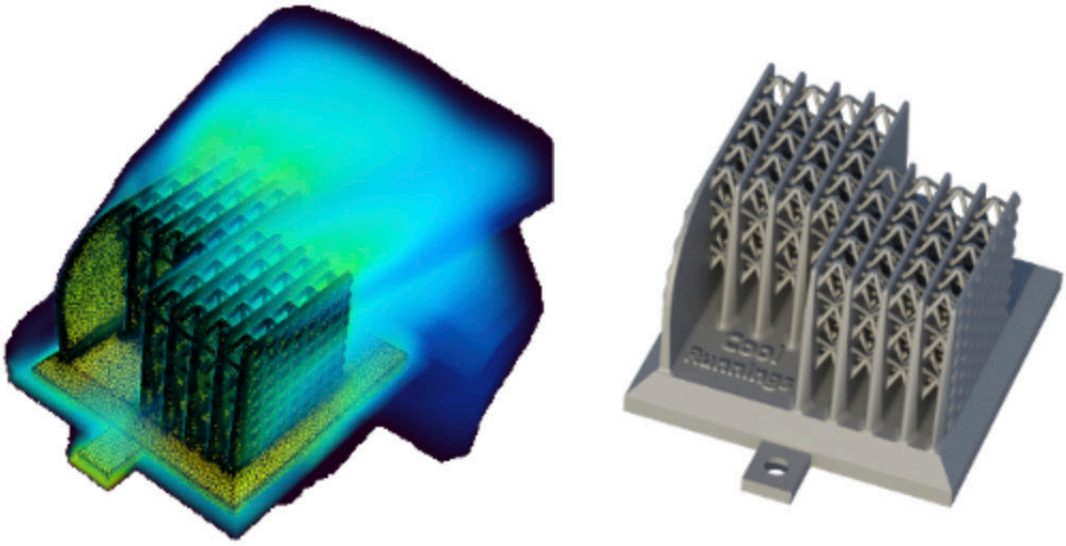

Figure 2: Winning Design - Technische Universität Berlin

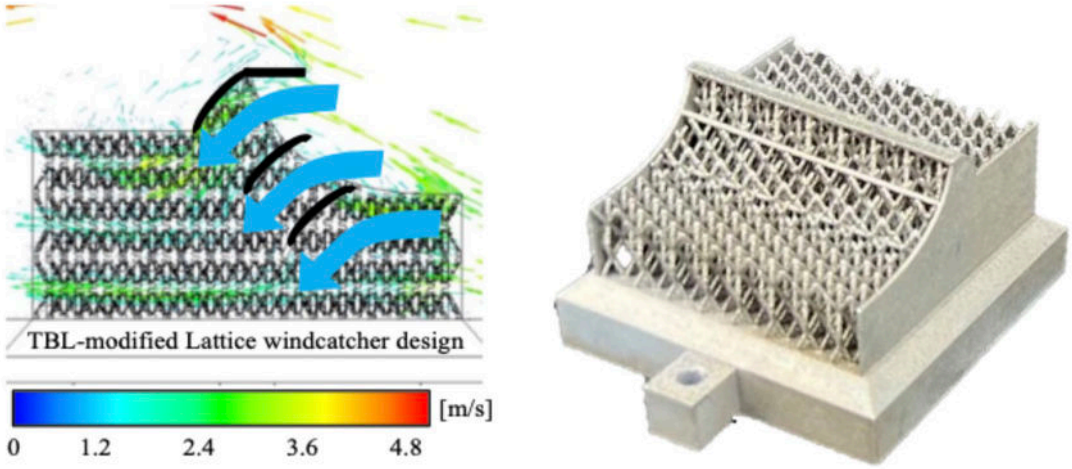

Figure 3: Runner-up – Michigan Technical University

Richard Chu ITherm Award for Excellence

Prof. Michael Ohadi was awarded the Richard Chu ITherm Award for Excellence. Prof. Ohadi is Minta Martin Professor of Mechanical Engineering and a co-founder of the Center for Environmental Energy engineering (CEEE) at the University of Maryland, College Park. For more than 25 years he has led an industrial consortium in Advanced Heat Exchangers and Process Intensification techniques with member companies from the U.S., Asia, and Europe. From 2016 to 2020, Ohadi served as Program Director (PD) at the U.S. department of energy, Advanced Research Project Agency-energy (ARPAE), where he led the development of programs in

thermal management and energy conversion systems, including lightweight and ultra-efficient electric motors, and associated power electronics for de-carbonization/electrification of aviation.

Proceedings

We are also pleased to announce that the ITherm 2022 Proceedings are available through IEEE Xplore Digital Library at https://ieeexplore.ieee.org/document/9899611. Papers appearing in the Table of Contents are available for access and download, along with listings of our Keynote Speakers, Tech Talks, Panels, Sponsors, and Exhibitors.

Sponsors and Exhibitors

ITherm 2022 was made possible by those of you who attended and by the generous support of our sponsors and exhibitors.

ITherm 2022 Organization Committee

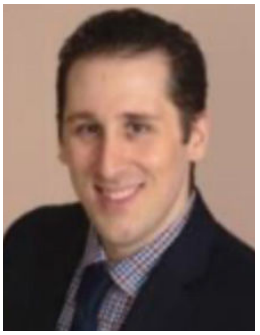

Dustin Demetriou, Ph.D.
IBM
General Chair

Satish Kumar, Ph.D.
Georgia Tech
Program Chair

Ashish Gupta, Ph.D.
Intel Corporation
Vice Program Chair

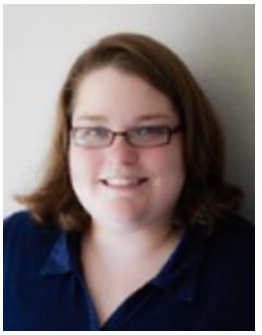

Amy Marconnet, Ph.D.
Purdue University
Communications Chair

ITherm 2023

We hope you will join us at the JW Marriott Grande Lakes, Orlando, FL May 30th-June 2nd, 2023, for ITherm 2023.

ITherm
ORLANDO, FL 2023

Is That Normal?

Ross Wilcoxon
Associate Technical Editor for *Electronics Cooling*
Collins Aerospace

Introduction

These columns on statistics began by describing the field of statistics as using the mathematical laws of probability to deal with data uncertainty [1]. Many statistical tools developed to apply probability do assume that data are drawn from a normally distributed population, in which the probability distribution function, f(x), of a population follows ***Equation {1}***.

$$f(x) = \frac{1}{\sigma\sqrt{2\pi}} e^{-\frac{1}{2}\left(\frac{x-\mu}{\sigma}\right)^2} \qquad \{1\}$$

where μ is the average of the population and σ is the standard deviation.

One may then ask, how do we assess a population if it does not have a normal distribution? There are methods for conducting statistical analyses on data that are not normal, one of which will be discussed in the next column. Before using these tools, it may be important to determine whether a data set should be modeled as having a normal distribution. This column will describe a few methods for assessing the accuracy of assuming that a given data set follows a normal distribution.

Data Sets

Two somewhat similar data sets will be used to illustrate different methods for assessing normality. These are both measurements of lab ambient temperature that were collected during thermal testing. Data Set A was collected during a material thermal conductivity test that lasted approximately 3.5 hours. Data Set B is the ambient temperatures measured during an extended reliability test that lasted for more than a year. These two data sets are shown in ***Figure 1***.

Both data sets show some variations in temperatures with average values that are nearly the same (24.3 and 24.5°C for A and B respectively). However, there are a few notable differences between the two sets. The range (maximum minus minimum) for Data Set A (<1°C) is much smaller than for Data Set B (~9°C). Given that Data Set B represents data over a time frame that is more than 3,000 times longer than Data Set A, it is not surprising that it exhibits a wider temperature range. Perhaps more importantly, Data Set B has some anomalous behavior, starting around day 300 with particularly low temperatures around day 360. Since this test was started in January, the temperature 'valley' around days 300-360 may be associated with the effects of weather - the lab was air-conditioned but has a fume hood to outside air.

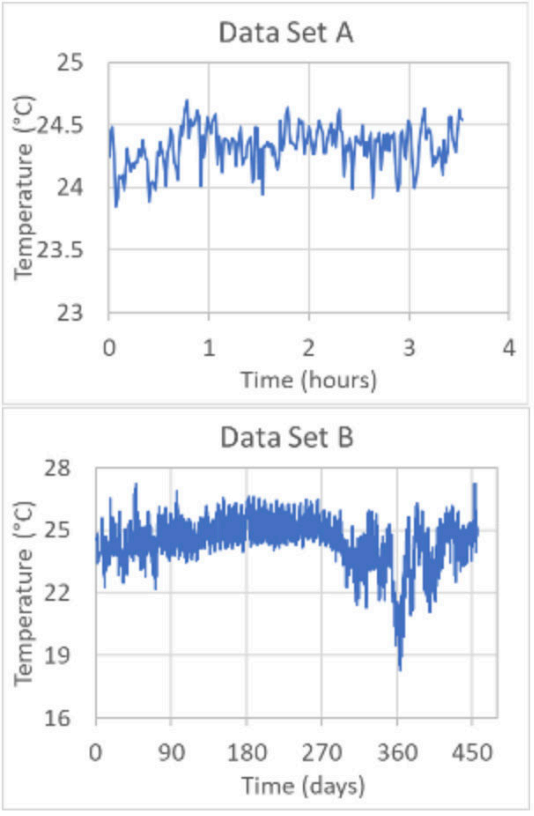

Figure 1: Data Sets for Analysis

Data Comparison

Table 1 shows statistical parameters calculated for the two different data sets. The first six rows in this table (in orange) show parameters that have been discussed in previous articles and should be familiar to the reader. The second column in the table indicates the Excel functions used to calculate the terms. In these functions, the term '(data)' indicates an array that comprises the data set being analyzed. As mentioned, the average values for the two data sets

are similar while the variance of B, in terms of the extreme values as well as the standard deviation, is much greater for Data Set B. The second group of results in the table (rows 7-10, in green) shows simple calculations that can provide insight into the characteristics of the distribution. The last two rows (in red) introduce two new functions that help quantify the normality of a data set. The terms in these last two groups are discussed later in this article.

Table 1: Statistical Comparison of Data Sets

Statistic	Excel Function	Set A	Set B
Mean (μ)	*=average(data)*	24.33	24.49
Median (Mdn)	*=median(data)*	24.34	24.59
Maximum	*=max(data)*	24.70	27.23
Minimum	*=min(data)*	23.85	18.27
# of samples	*=count(data)*	213	10945
Stand dev (σ)	*=stdev(data)*	0.17	1.19
Range (Δ)	*=max-min*	0.85	8.95
Δ/σ	*=delta/sigma*	5.05	7.53
σ/μ	*=sigma/mean*	0.7%	4.9%
|μ/Mdn - 1|	*=abs(μ/Mdn-1)*	0.06%	0.39%
Kurtosis	*=kurt(data)*	-0.06	2.36
Skew	*=skew(data)*	-0.45	-1.09

One visual approach for assessing a data set's distribution is to generate a frequency plot, such as those shown in ***Figure 2***. These were generated by breaking the range of values for each data set into 20 bins (with a bin size of range/20). The number of measurements less than or equal to the value at the center of the bin was divided by the total number of measurements for that data set. These results are plotted for each bin. In addition, the plots show the cumulative normal distribution for each population (calculated using the Excel function '=norm.dist(x,μ,σ,true)', where the bin-center values were used for each x-value).

The two plots show that the cumulative binned data generally match the calculated normal distributions fairly well. Data Set B has a much longer tail than Set A, due to the low-temperature spike seen in the data around day 360. Other than the long tail in the plot for Set B and a few local differences between the heights of some bars and the normal distribution line, the plots in ***Figure 2*** don't provide any compelling indication that either data set is not normally distributed.

Q-Q Plots

A better approach for comparing the data to a normal distribution is a quantile-quantile (Q-Q) plot. In a Q-Q plot, x-values are determined by first finding the rank (low to high) of each data point and dividing it by the number of samples to estimate a probability. For example, the minimum value of Set A of 23.85°C would have a rank of 1 and the probability for that measurement would then

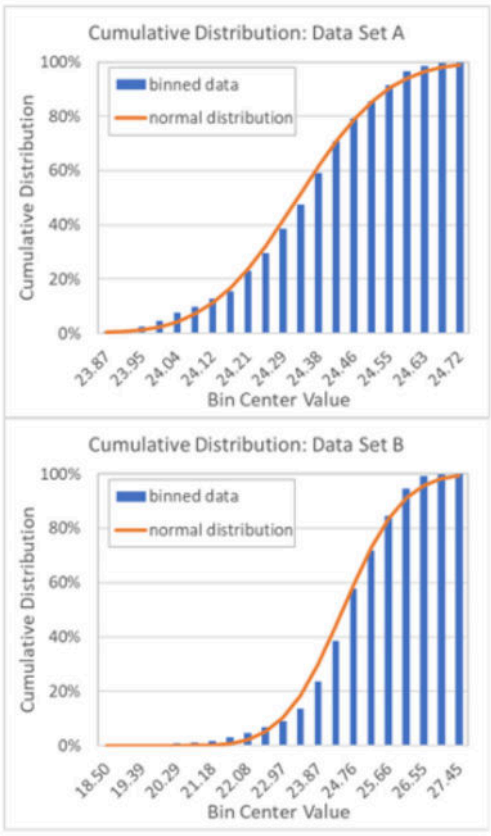

Figure 2: Cumulative Probability Distributions for Data Sets

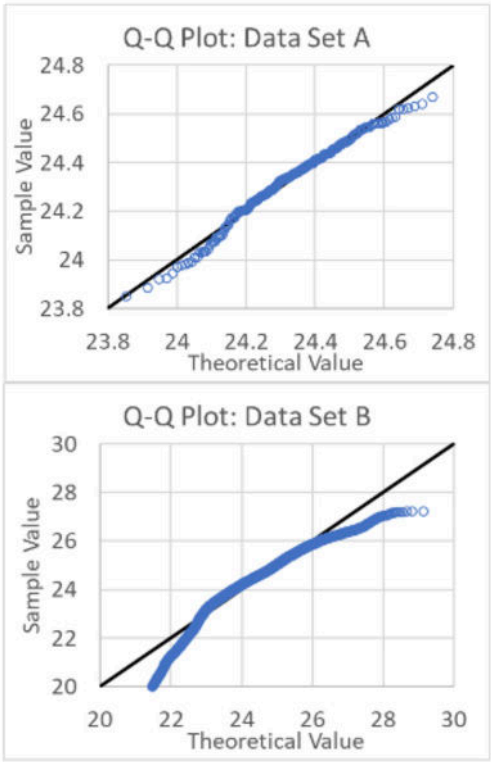

Figure 3: Q-Q Plots for Data Sets

be 1/213 (since the data set was comprised of 213 measurements). The x-value for that data point is calculated by finding the value in a normal distribution corresponding to that probability value. Using the mean and standard deviation for Data Set A (24.33 and 0.17, respectively as shown in ***Table 1***), the x-value corresponding to the minimum term with a rank of 1 would be calculated in Excel as '=norm.inv((1/213), 24.33, 0.17)' = 23.89°C. The y-value would be the actual measured value of 23.85°C. This is done for each measured data point; the resulting Q-Q plots, including reference lines of x=y, are shown in ***Figure 3***.

If a data set had a perfect normal distribution, its Q-Q plot would exactly follow the x=y line. ***Figure 3*** reveals some deviations for both data sets, but the plot for Data Set B does exhibit much larger deviations at the extremes (the lowest and highest values) than Data Set A. While not perfect, the Q-Q plot provides a visual method to assess how well a population conforms to a normal distribution.

Standard Deviation Normalization

Comparing a data set's standard deviation to its mean and range can roughly indicate how well it conforms to a normal distribution. A general rule of thumb is that 95% of a normal distribution is within 2 standard deviations of the mean (a total range of ±2 = 4 total standard deviations) and 99.7% is within ±3 standard deviations. Assuming that the minimum and maximum values are roughly equal distance from the mean, then it is reasonable to assume that 5% (1-95%) of a normal distribution would have a range/standard deviation (Δ/σ) value of 4 and 0.3% would have Δ/σ of 6. The value of $\Delta/\sigma = 5.05$ for Data Set A would be expected to occur for ~1% of the data in a normal distribution[1]. In comparison, the probability of seeing the Set B result of $\Delta/\sigma=7.53$ is much smaller at 0.017%. While that value is small, given the large sample size in Set B, this is not necessarily proof that the population is not normal.

The ratio of the standard deviation to average, σ/μ, does not necessarily indicate whether a set of data is normally distributed, but the substantial difference between the two sets (0.7% for Set A and 4.9% for Set B) does indicate that the two populations have different characteristics. Likewise, the difference between the means and medians for the two data sets, as expressed with the term $|\mu - Mdn|$-1, does imply that the two populations are different.

Kurtosis and Skew

Kurtosis and skew are quantified parameters that help describe how well a given distribution conforms to a normal distribution. As shown in ***Figure 4***, kurtosis indicates whether a distribution is vertically compressed or expanded relative to a normal distribution. A positive kurtosis corresponds to a distribution with very small tails, which leads to more of the population being centered close to the mean. A negative kurtosis has larger tails than expected. Skew indicates an asymmetric distribution that has a larger tail on one side. A distribution with a positive skew is skewed to the right (larger tail on the right) with a mean that is larger than the median. A negative skew has a larger tail on the left and the mean is smaller than the median.

Distributions with 'excess kurtosis' with an absolute value in the range of 0-0.5 are reasonably normal. Distributions with an absolute value of skew of 0-0.5 are considered symmetric and normally distributed. Absolute values of skew between 0.5 and 1 are 'slightly skewed' and distributions with absolute skew greater than 1 are extremely skewed [2].

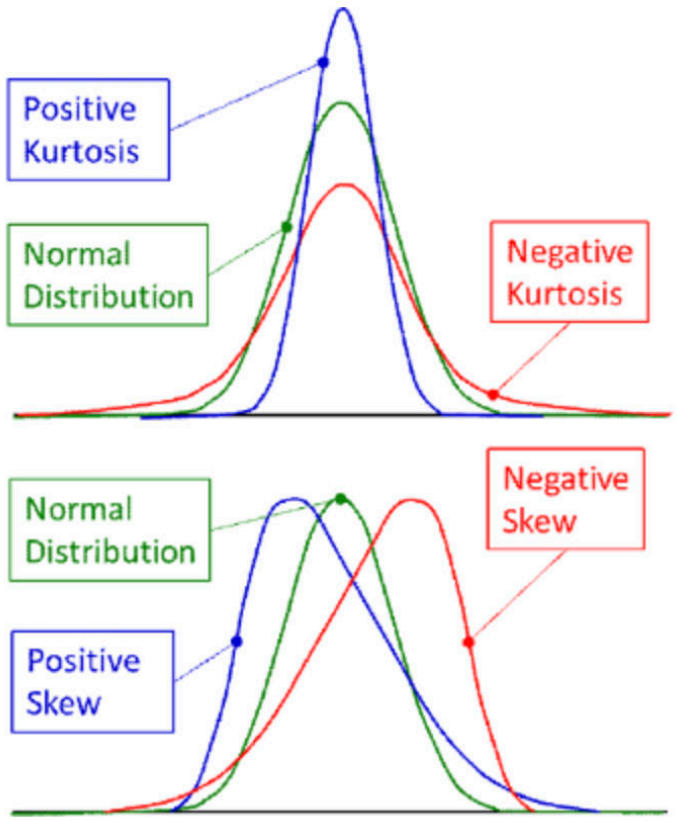

Figure 4: Kurtosis and Skew

For the data considered in this article, Data Set A had kurtosis and skew of -0.06 and -0.45 respectively. With these values, that data set would be considered normally distributed. In comparison, Data Set B had kurtosis and skew values of 2.36 and -1.09 respectively. Both values indicate that these data are not well described with a normal distribution. Specifically, the data have a large tail to the left and a higher fraction of measurements near the average than would be expected for the calculated standard deviation. Both of these results are a result of the cold temperature spike that occurred around Day 360, which increased the calculated standard deviation and also generated a long tail on the left (low temperature) side of the distribution.

[1] Calculated in Excel using =norm.dist((5.05/2, 0,1,true), because the x-value in this calculation is the distance from the mean divided by the standard deviation, it is for a normalized distribution with a mean of 0 and standard deviation of 1.

Summary

Many statistical analysis tools have been developed using the assumption that data are taken from populations with a normal distribution. In reality, real data are almost never normally distributed but instead only approximate it with varying degrees of success. This article has discussed a few methods for assessing data to determine how close, or far, it deviates from the normal distribution assumption.

If the distribution of a data set substantially differs from normal, alternate statistical analysis approaches may be needed to make assessments. The next article in this series will discuss a method for comparing two data sets to determine whether they are statistically different using an approach that does not assume a normal distribution. This technique is this author's favorite statistical test, for reasons that will become apparent once it is described.

References

[1] Ross Wilcoxon, "Statistics Corner: Probability", Electronics Cooling Magazine, Spring 2020, https://www.electronics-cooling.com/wp-content/uploads/2020/03/Electronics-Cooling_Spring-2020.pdf

[2] Sufana Gawali, "Shape of data: Skewness and Kurtosis", Analytics Vidhya, https://www.analyticsvidhya.com/blog/2021/05/shape-of-data-skewness-and-kurtosis/


Call for Authors
and Contributors!
Want to be a part of the next issue of Electronics Cooling? Have an article or blog post you'd like to write for Electronics-Cooling.com?
Let us know at
editor@electronics-cooling.com
electronics COOLING
www.Electronics-Cooling.com

Index of ADVERTISERS

Electronics Cooling
1000 Germantown Pike,
Plymouth Meeting, PA 19462

t: 484.688.0300
e: info@electronics-cooling.com
w: www.electronics-cooling.com
page: 35

Ellsworth Adhesives
W129 N10825 Washington Drive
Germantown, WI 53022

t: (877) 454-9224
e: info@ellsworth.com
w: www.ellsworth.com
page: 5

LECTRIX
1000 Germantown Pike
Plymouth Meeting, PA 19462

t: (484) 688-0300
e: info@lectrixgroup.com
w: www.lectrixgroup.com
page: 37

SEMI-THERM
3287 Kifer Road
Santa Clara, CA 95051

t: (408) 840-2354
w: www.semi-therm.org
page: 11

SIEMENS Digital Industries Software
8005 SW Boeckman Road
Wilsonville, OR 97070

t: (800) 592-2210
e: www.plm.automation.siemens.com/global/en/contact-us.html
w: www.plm.automation.siemens.com/global/en/
page: 2


Break the same old pattern.
Problem First. Product Last.
Content | Data | Marketing Technology
LECTRIX®
Digital Marketing for the B2B Electronics Industry
1.484.688.0300 | info@lectrixgroup.com
www.lectrixgroup.com